Performance Evaluation of GNSS Meta-Signals Under Multipath Environment

Robin Duprat, *TéSA and ENAC, Toulouse, France*
Emile Ghizzo, Paul Thevenon, *ENAC, Toulouse, France*
Lorenzo Ortega, *IPSA and TéSA, Toulouse, France*
Sébastien Roche, Margaux Bouilhac, *Thales Alenia Space, Toulouse, France*
François-Xavier Marmet, *Centre National d'Etudes Spatiale, Toulouse, France*

BIOGRAPHY

Robin Duprat is first-year PhD student at TéSA and ENAC. He received a master's degree in aeronautics from ENAC in 2023. His Ph.D. research focuses on GNSS meta-signal processing.

Emile Ghizzo received a master's degree in aeronautics from ENAC in 2021 and a master's degree in aerospace systems specializing in navigation and telecommunications from ISAE SUPAERO in Toulouse. He obtained a Ph.D. degree in 2025 in telecomunication at ENAC, focusing on GNSS signal processing and jamming and spoofing detection. His current activities are GNSS reflectometry and GNSS tracking.

Paul Thevenon graduated as electronic engineer from Ecole Centrale de Lille in 2004 and obtained in 2007 a research master at ISAE in space telecommunications and a Ph.D. degree in 2010 in signal processing at ENAC. From 2010 to 2013, he was employed by CNES to supervise GNSS research activities and measurement campaigns. Since July 2013, he has been employed by ENAC as Associate Professor. His current activities are GNSS signal processing and GNSS precise positioning algorithms.

Lorenzo Ortega defended his doctoral thesis at the National Polytechnic Institute of Toulouse (INPT) in November 2019. He then completed a postdoctoral fellowship co-funded by TéSA and ISAE-Supaero, focusing on robust statistics applied to navigation. In late 2021, he joined IPSA as an Associate Professor and became affiliated with TéSA as a research laboratory. In March 2025, he obtained his accreditation to direct research (HDR) from the University of Toulouse III – Paul Sabatier. His research focuses primarily on statistical signal processing and digital communications, with applications in satellite communications, localization, navigation, and remote sensing.

Sebastien Roche is a GNSS Studies Engineer at Thales Alenia Space Toulouse. He graduated as an aeronautical engineer from ISAE-ENSICA in 2010. He obtained a PhD degree in 2013 from the University of Toulouse by studying robust phase tracking algorithms. Since then, his activities have mainly focused on GNSS signal processing.

Margaux Bouilhac was graduated as telecommunications and network engineer from ENSEEIHT Toulouse in 2015 with a specialization in Space Communication Systems. She joined the navigation department of Thales Alenia Space - France in 2021, as a GNSS signal processing engineer. She is currently working on GNSS precise algorithms, in both the tracking and PVT stages.

François-Xavier Marmet is a Radionavigation Expert with CNES, the French Space Agency. He has been with CNES for 12 years, where he has addressed a broad range of PNT topics. Most recently, he has been involved in Galileo 2nd Generation through participation in several European working groups, and he is leading the development of several spaceborne GNSS receivers.

ABSTRACT

Global Navigation Satellite Systems (GNSS) are fundamental for positioning, navigation, and timing (PNT), playing a crucial role in next-generation intelligent transportation systems and safety-critical applications. However, achieving precise PNT solutions in challenging environments remains a significant challenge. Under ideal conditions, carrier-phase-based techniques such as Real-Time Kinematics (RTK) and Precise Point Positioning (PPP) enable high-precision positioning. However, their accuracy heavily depends on the quality of phase observables, which can be degraded in harsh environments, such as urban canyons or interference-prone scenarios. A promising alternative is the use of large-bandwidth signals, which enhance resolution and improve code-based observables. This can be achieved through high-order Binary Offset Carrier modulations or GNSS meta-signals. This study investigates the fundamental performance limits of time delay and Doppler estimation for such signals in challenging scenarios, particularly in the presence of multipath interference, where signal reflections significantly impact receiver performance. Characterizing multipath effects is critical for the next generation of PNT applications, as it directly

influences the robustness of GNSS solutions. To analyze these effects, we derive the Cramér-Rao Lower Bound (CRB) for time-delay and Doppler estimation under a signal model where one specular multipath degrades GNSS receiver performance. This case considers that the receiver is aware of the multipath and applies countermeasures. In the second case, we assume that the receiver is unaware of the multipath, for which we derive the Misspecified CRB (MCRB). The MCRB quantifies the performance degradation in standard GNSS receivers due to unmodeled multipath interference. We validate these theoretical bounds by comparing them with state-of-the-art estimation algorithms. Our results demonstrate the significant performance improvements achievable in harsh conditions using metasignals such as Galileo E5a + E5b or GPS L2 CM + L5, compared to legacy signals such as GPS L1 C / A.

I. INTRODUCTION

Since the proposal of Binary Offset Carrier (BOC) modulation (Betz, 2001), the GNSS community has shown significant academic interest in developing advanced modulations to improve positioning accuracy. In particular, various BOC-based modulation variants have been suggested in recent years (Ortega et al., 2018; Paonni and Bavaro, 2013; Rebeyrol, 2007; Rodríguez, 2008), some of which have been adopted in next-generation satellite navigation systems, such as Galileo. Alongside these BOC modifications, research has also focused on signals transmitted over multiple frequencies. A key example is the AltBOC modulation (Issler et al., 2010; Lestarquit et al., 2008), implemented in the Galileo satellite navigation system. As interest in multi-frequency modulations grew, the concept of the Meta-Signal emerged (Paonni et al., 2014), leading to numerous studies exploring its advantages. In particular, (Ortega et al., 2020) analyzed the accuracy of estimating time-delay of various metasignals in an open sky scenario. Subsequent works, such as (Borio, 2023) and (Borio and Susi, 2024), introduced realistic implementations of meta-signals, while (Borio, 2024) generalized the concept to multiple signals, extending it beyond just two frequencies. Despite these advancements, one of the key theoretical gaps in the study of meta-signals remains the analysis of their performance in multipath environments. Addressing this issue is the primary contribution of this article.

As in other technologies such as radar, sonar, and digital communications, accurately estimating time delay and Doppler shift is of critical importance. In the GNSS domain, receivers extract this information from satellite broadcast signals to form GNSS observables (code, phase, Doppler measurements) that are then processed to compute the positioning, navigation, and timing (PNT) solution. Therefore, assessing the accuracy of these estimates is essential to evaluate the performance and limitations of GNSS-based applications. To achieve this, we commonly use the Conditional Signal Model (CSM) (Medina et al., 2020; Stoica and Nehorai, 1990), which treats the time delay and Doppler as unknown deterministic parameters. This model facilitates the derivation of the Cramér-Rao Bound (CRB), providing a fundamental benchmark for the best achievable estimation performance under the assumption of unbiased estimators.

Under the assumption of a Gaussian observation model, the derivation of these bounds is usually based on the Slepian-Bangs formula (Kay, 1993; Ottersten et al., 1993). However, when addressing multi-source signal models, such as in multipath scenarios, deriving the CRB becomes considerably more complex. Significant CRB formulations have been developed for various radar domain applications, including extended targets (Lubeigt et al., 2023; Zhao and Huang, 2016) and GNSS-R altimetry (Camps et al., 2014; Germain and Ruffini, 2006; Ribot et al., 2016). A key contribution to this field was made in (Lubeigt et al., 2020), where the authors derived a closed-form expression for the CRB of the time-delay and Doppler in the context of dual-source (specular multipath) and under the assumption of band-limited signal. This case assumes that the receiver is aware of the multipath and applies appropriate countermeasures. To validate the CRB implementation, the Conditional Maximum Likelihood Estimator (CMLE) is often used, as it is well known to be asymptotically unbiased and efficient as a function of the signal-to-noise ratio (Renaux et al., 2006; Stoica and Nehorai, 1990). In other words, its mean square error converges to the CRB as the noise conditions improve or the integration time increases. These characteristics make CMLE a valuable tool for validating CRB expressions, as demonstrated in studies such as (Lubeigt et al., 2020; Ortega et al., 2020). However, in the context of dual-source (multipath) signals, CMLEs can be computationally intensive, which often leads practitioners to seek more efficient alternatives. Numerous solutions have been suggested in the literature to mitigate this computational burden. In this article, we focus on the CLEAN Relax algorithm, also known in the GNSS community as the Multipath Estimating Delay Lock Loop (MEDLL) (Kaplan and Hegarty, 2017). For single multipath scenarios, the CLEAN Relax algorithm replaces the computationally expensive 2-dimensional search for parameters with two recursive 1-dimensional searches: first, it estimates the parameters corresponding to the Line-of-Sight (LOS) signal, and then it estimates the parameters for the multipath component once the LOS has been compensated. Although this method provides a good approximation of the CMLE in most cases, it struggles to accurately estimate the parameters when both signals arrive nearly simultaneously, resulting in an identifiability problem.

Additionally, an important consideration when discussing multipath is the behavior of standard receivers, where the incoming signal is typically treated as only the direct signal, rather than as a combination of both direct and multipath components. In this case, the single source (standard) CMLE becomes biased due to the misspecification of the signal model. In such a case, this estimator is referred to as the misspecified CMLE. To accurately characterize the asymptotic performance of the CMLE and, consequently, the impact of multipath, it is essential to apply the misspecified estimation theory (Fortunati et al., 2017;

Fortunati and Ortega, 2024). This framework provides a means of quantifying both the bias and the variance of the estimation, the variance being determined by the misspecified Cramér-Rao Lower Bound (MCRB) (Lubeigt et al., 2023).

1. Contributions

This article aims to characterize the performances of meta-signals (Galileo E5 meta-signal (AltBOC) and GPS L2 CM + L5 meta-signal) in a multipath context. To do so, we derive the CRBs of timing, phase, and frequency estimation under multipath environment. Different models such as well-specified and misspecified models are considered. These bounds are compared with the mean squared error (MSE) obtained from the simulated algorithms using two estimators: Maximum Likelihood Estimator and CLEAN Relax Estimator. To identify the benefits of using meta-signals, these performances are compared with GPS L1 C/A performances. Regarding the existing literature on the derivation of Cramér-Rao lower bounds (Lubeigt et al., 2020) and misspecified CRB (Lubeigt et al., 2023) for GPS L1 C/A, the latter can be used to validate the estimation algorithm before applying them on GNSS meta-signals.

2. Notation

The adopted notations are as follows: scalars are represented by italic lowercase characters as in b; vectors are represented by bold lowercase characters as in $\mathbf{b}$; matrices are represented by bold uppercase characters as in $\mathbf{B}$; the true signal parameters are represented with a bar as in $\bar{b}$; the transpose operation is indicated by the superscript ^{T}; the conjugate transpose by the superscript ^{H}; the conjugate operation by the superscript *; $\mathbf{I}_n$ represents the identity matrix of dimension n; $\Re\{\cdot\}$ and $\Im\{\cdot\}$ refer to the real part and the imaginary part.

3. Organization

Section II provides a detailed description of the signal model. In Section III, the well-specified dual-source CRB is derived, and the dual-source CMLE and CLEAN Relax estimators are introduced. Section IV presents the misspecified signal model, derives the associated bias, and derives the MCRB expressions. Additionally, it introduces the misspecified CMLE, which asymptotically converges to the MCRB. Section V presents the simulation process that is performed in the next section. Section VI evaluates the accuracy and robustness of meta-signals, comparing their performance against legacy signals. Finally, conclusions are drawn in Section VII.

II. SIGNAL MODEL

We consider the transmission of a band-limited GNSS signal $s\left(t\right)$ over a carrier frequency f_c (such that $\lambda_c = c/f_c$, with c the speed of light in vacuum), from a transmitter T (GNSS satellite) to a receiver R (GNSS receiver). We assume that the transmitter and receiver are in a uniform linear motion, with their respective positions evolving as $\mathbf{p}_T(t) = \mathbf{p}_T(0) + \mathbf{v}_T t$ and $\mathbf{p}_R(t) = \mathbf{p}_R(0) + \mathbf{v}_R t$. We also consider that the relative velocity between them is given by $\mathbf{v} = \mathbf{v}_T - \mathbf{v}_R$. The radial distance between the transmitter T and the receiver R is defined as $p_{TR}(t) = \|\mathbf{p}_T(t - \tau_{\text{true}}(t;\bar{\boldsymbol{\eta}})) - \mathbf{p}_R(t)\|$, where $\tau_{\text{true}}(t;\bar{\boldsymbol{\eta}})$ represents the time delay as a function of time and the true parameters, with $\bar{\boldsymbol{\eta}} = [\bar{\tau}, \bar{b}]^T \in \mathbb{R}^2$ being the true delay and the Doppler effect. On the radial from the transmitter to the receiver, a unitary vector $\mathbf{u} = \dfrac{\mathbf{p}_T(t - \tau_{\text{true}}(t;\bar{\boldsymbol{\eta}})) - \mathbf{p}_R(t)}{p_{TR}(t)}$ is placed. This distance is used to compute the ranging equation defined as:

$$p_{TR}(t;\bar{\boldsymbol{\eta}}) = c\tau_{\text{true}}(t;\bar{\boldsymbol{\eta}}) \tag{1}$$

In this context, we consider the case where the propagation delay $\tau_{\text{true}}(t;\bar{\boldsymbol{\eta}})$ can be approximated, within the observation time, by a first-order distance-velocity model.

$$p_{TR}\left(t;\bar{\boldsymbol{\eta}}\right) = \|\mathbf{p}_T\left(t - \tau_{\text{true}}(t;\bar{\boldsymbol{\eta}})\right) - \mathbf{p}_R\left(t\right)\| = c\tau_{\text{true}}(t;\bar{\boldsymbol{\eta}})\left(t\right) \simeq c\left(\bar{\tau} + \bar{b}t\right) \tag{2}$$

where $\bar{\tau} = \dfrac{\|\mathbf{p}_T(0) - \mathbf{p}_R(0)\|}{c}$ and $\bar{b} = \dfrac{\mathbf{u}\cdot\mathbf{v}}{c} = \dfrac{\|\mathbf{v}\|\cos((\mathbf{u},\mathbf{v}))}{c}$. Under the narrowband assumption, i.e., $B \ll f_c$, the Doppler effect on the baseband signal $s\left(t\right)$ can be considered negligible, leading to the approximation $s\left((1-\bar{b})(t-\bar{\tau})\right) \approx s\left(t-\bar{\tau}\right)$. Note that the dilation term $(1-\bar{b})$ is induced by the Doppler effect.

In this particular case, for an ideal transmitter, propagation channel, and receiver, the noise-free signal at the output of the receiver's Hilbert filter (I/Q demodulation) is given by (Medina et al., 2020):

$$f\left(t;\bar{\boldsymbol{\theta}}\right) = \bar{\alpha}s\left(t-\bar{\tau}\right)e^{-j2\pi f_c\bar{b}(t-\bar{\tau})}, \tag{3}$$

where $\bar{\alpha} = \bar{\rho}e^{j\bar{\phi}}$ and $\bar{\boldsymbol{\theta}} = [\bar{\boldsymbol{\eta}}^T, \bar{\rho}, \bar{\phi}]^T$, with $\bar{\rho}$ and $\bar{\phi}$ representing the magnitude and phase of the complex amplitude $\bar{\alpha}$. Finally, if we consider the acquisition of $N = |N_2 - N_1 + 1|$ samples separated by a time interval $T_s = 1/f_s$, with f_s the sampling frequency, then the discrete vector signal model is given by

$$\mathbf{f}(\bar{\boldsymbol{\theta}}) = \bar{\alpha}\mathbf{a}\left(\bar{\boldsymbol{\eta}}\right) = (\ldots, f(nT_s; \bar{\boldsymbol{\theta}}) = \bar{\alpha}s(nT_s - \bar{\tau})e^{-j2\pi f_c \bar{b}(nT_s - \bar{\tau})}, \ldots)^\top \tag{4}$$

where $n \in [1, N]$ represents the sample index.

In complex environments such as urban canyons, a GNSS receiver may capture not only the Line-of-Sight (LOS) signal but also multiple reflected and diffracted copies from the receiver due to interactions with surrounding surfaces such as buildings, water bodies, and vehicles. These unwanted Non-Line-of-Sight (NLOS) signals, collectively known as multipath, can degrade the receiver's performance. The multipath is considered a form of self-interference (Dovis, 2015), posing a persistent challenge in urban navigation due to its significant impact. The issue of multipath, a key barrier to precise positioning in urban settings, is extensively covered in the specialized literature on GNSS, including (Kaplan and Hegarty, 2017, Ch. 9.5), (Teunissen and Montenbruck, 2017, Ch. 15), and (Morton et al., 2021, Ch. 22).

A simple approach to understand the multipath problem is to consider a scenario where the receiver antenna captures both the LOS and a single specular reflection. This reflection can originate from an object that occupies a significant portion of the cross section of the first Fresnel zone (Beckmann and Spizzichino, 1987). The first Fresnel zone is an ellipsoidal region surrounding the LOS path between a transmitting and receiving antenna, including all points where the total path length to both antennas is longer than the LOS distance by half a wavelength (Teunissen and Montenbruck, 2017). Under this assumption, and disregarding thermal noise, the LOS signal (indexed as 0), affected by a single multipath component (indexed as 1), at the output of Hilbert's filter, can be written as:

$$f(t; \bar{\boldsymbol{\theta}}) = \bar{\rho}_0 e^{j\bar{\phi}_0} s(t - \bar{\tau}_0)e^{-j\omega_c \bar{b}_0(t-\bar{\tau}_0)} + \bar{\rho}_1 e^{j\bar{\phi}_1} s(t - \bar{\tau}_1)e^{-j\omega_c \bar{b}_1(t-\bar{\tau}_1)} \tag{5}$$

The set of *true* parameters is given by $\bar{\boldsymbol{\theta}} = [\bar{\boldsymbol{\theta}}_0, \bar{\boldsymbol{\theta}}_1] = [\bar{\tau}_0, \bar{b}_0, \bar{\rho}_0, \bar{\Phi}_0, \bar{\tau}_1, \bar{b}_1, \bar{\rho}_1, \bar{\Phi}_1]^\top$. For this particular signal model, it is useful to define several parameters that fully characterize the multipath scenario.

- Excess time delay or path separation: $\Delta\bar{\tau} = \bar{\tau}_1 - \bar{\tau}_0$, which is always positive since an NLOS path is necessarily longer than the LOS path.
- Multipath-to-direct amplitude ratio (MDR): MDR $= \bar{\rho}_1/\bar{\rho}_0$, typically less than 1, as reflections generally attenuate the signal.
- Phase difference: $\Delta\bar{\phi} = \bar{\phi}_1 - \bar{\phi}_0$.

Finally, assuming that the receiver is affected by additive noise, typically modeled as a zero-mean Gaussian random process, our signal model is described by the following nonlinear regression model.

$$\mathbf{x} = \mathbf{A}(\bar{\boldsymbol{\eta}}_0, \bar{\boldsymbol{\eta}}_1)\bar{\boldsymbol{\alpha}} + \mathbf{w},\ \mathbf{w} \sim \mathcal{CN}(0, \bar{\sigma}_n^2 \mathbf{I}_N)\ , \tag{6}$$

with $\bar{\sigma}_n^2$ the variance of the noise following a complex normal distribution and $\mathbf{I}_N$ a diagonal matrix of dimension N. Moreover,

$$\begin{aligned}
&\mathbf{x}^T = (\ldots,\ x(nT_s),\ \ldots)\ , \\
&\mathbf{A}(\bar{\boldsymbol{\eta}}_0, \bar{\boldsymbol{\eta}}_1) = [\mathbf{a}_0,\ \mathbf{a}_1]\ , \\
&\mathbf{a}_i^T = \left(\ldots,\ s(nT_s - \bar{\tau}_i)e^{-j\omega_c \bar{b}_i(nT_s - \bar{\tau}_i)},\ \ldots\right)\ , \\
&\bar{\boldsymbol{\alpha}}^T = \left(\bar{\rho}_0 e^{j\bar{\phi}_0},\ \bar{\rho}_1 e^{j\bar{\phi}_1}\right)\ , \\
&\mathbf{w}^T = (\ldots,\ w(nT_s),\ \ldots)\ .
\end{aligned}$$

1. Meta-Signal definition

In this paper, we define a meta-signal as a set of conventional GNSS signals (e.g. GPS L2 CM or Galileo E5a). Even if the literature mentions the possibility of creating meta-signals from multiple conventional signals (Borio, 2024), the scope of this paper only considers meta-signals with two conventional signals (eg. GPS L2CM + L5 and or Galileo E5). All conventional signals considered in this article (Galileo E5a / E5b, GPS L2CM / L5) are modulated by BPSK. However, the resulting meta-signals can be considered as signals generated with ALTBOC (Alternate Binary Offset Carrier) and ALTLOC (Alternate Linear

Offset Carrier) modulations (Ortega et al., 2020). The ALTLOC modulation considered in this paper is based on pure sin and cosine subcarriers. However, this modulation is known to have a non-constant envelope when multiplexing only the code components (Lestarquit et al., 2008). Thus, in order to have the high power amplifier of the emitter working at saturation, the products of the intermodulation code must be integrated into the signal (Paonni et al., 2014). At the receiver level, these intermodulation codes will appear as new secondary lobes in the signal power spectral density, which are placed at odd factors of the emitter sampling frequency. The bandwidth of these lobes will then be the least common multiple of the chip rates of the code components.

ALTBOC modulations are represented as ALTBOC(p, q, w) where the signal subcarrier frequency is $f_{\text{sub}} = p \cdot f_0$, the lower code chip rate (corresponding to the signal located at $f_c - f_{\text{sub}}$, f_c being the signal carrier frequency) is $f_{\text{chip},L} = q \cdot f_0$ and the upper code chip rate (corresponding to the signal located at $f_c + f_{sub}$) is $f_{\text{chip},U} = w \cdot f_0$, $f_0 = 1.023$ MHz. The subcarrier frequency is defined as the semi-difference of the frequencies of the composite signals (Borio, 2023). Then, an additional piece of information, $BW = b \cdot f_0$ is added to represent the receiver bandwidth is added in the ALTLOC(p, q, w, b) representation. Therefore, the set of meta-signals used in this article are generated with the following characteristics and summarized in Table 1:

- Galileo E5, generated as an ALTBOC(15,10) with $f_c = 1191.795$ MHz. For the specific case of Galileo, which is a symetrical ALTBOC signal, $q = w = 10$.
- GPS L2CM + L5, referred to as GPS L2-L5, generated as an ALTLOC(25,10,1,75) with $f_c = 1202,025$ MHz.

The power spectral densities of the ALTBOC and ALTLOC modulation are presented in Figure 1.

Conventional GNSS signals	Carrier frequency	GNSS meta-signal	Carrier and subcarrier frequency
GPS L2 CM	$f_c = 1227.60$ MHz	GPS L2 CM + L5	$f_c = 1202.025$ MHz
GPS L5	$f_c = 1176.45$ MHz		$f_{\text{sub}} = 25.575$ MHz
Galileo E5a	$f_c = 1176.45$ MHz	Galileo E5	$f_c = 1191.795$ MHz
Galileo E5b	$f_c = 1207.14$ MHz		$f_{\text{sub}} = 15.35$ MHz

Table 1: Meta-signal simulation plan

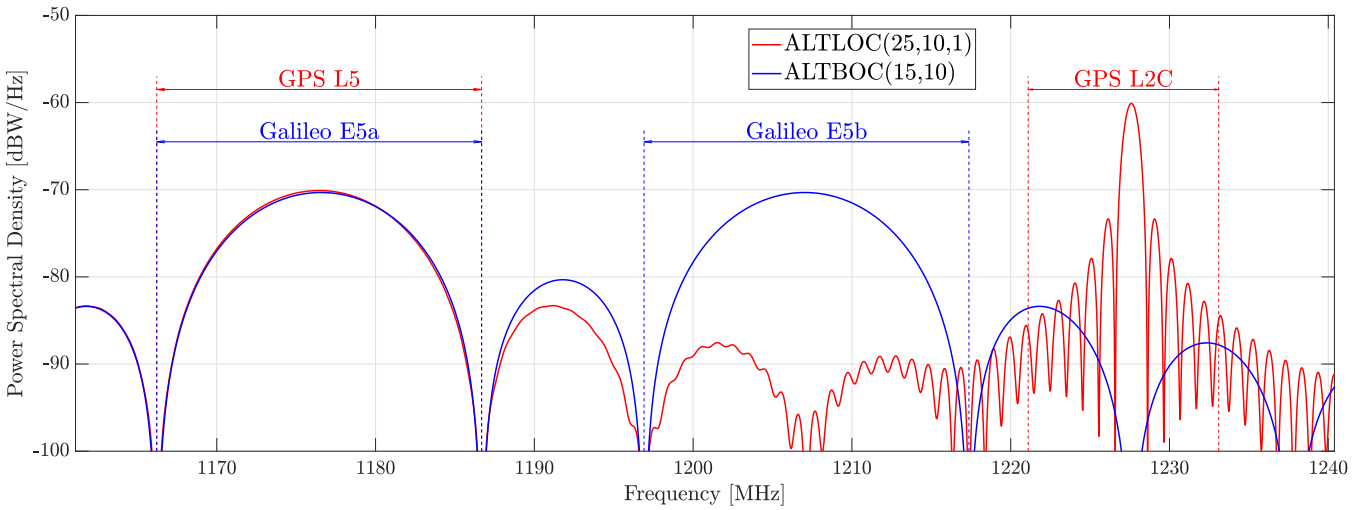

Figure 1: GPS L2C + L5 (red) and Galileo E5 (blue) power spectral densities

2. Multipath parameters assumptions on Meta-signals

In this paper, it is assumed that the meta-signal is uniformly impacted by the delay and the Doppler effect. This means that both conventional signals forming a meta-signal are delayed by the same delay and affected by the same Doppler effect. Indeed, it can be assumed that for a meta-signal under standard conditions, each of the conventional GNSS signal components may not be affected by the same delay and Doppler effect. Indeed, several sources, such as hardware biases in the satellite vehicle, ionosphere, or the reflection surface for a NLOS signal, may induce different delay and Doppler effect with respect to the conventional component of the meta-signal. That is why a more accurate approach might be to consider a specific delay and Doppler effect per meta-signal component. However, such a sophisticated model is outside the scope of this contribution and could be kept for future improvements.

III. MULTIPATH PERFORMANCE ESTIMATION UNDER WELL-SPECIFIED SIGNAL MODEL

In the literature, the Multipath Error Envelope (MPEE) is an easy-to-handle tool to assess the robustness of the signal to multipath (Teunissen and Montenbruck, 2017, Chapter 15). However, (Lubeigt et al., 2022) shows that this method has notable limitations, particularly when assessing parameter estimation performance. Specifically, the MPEE does not provide an estimate of an estimator's variance and therefore becomes uninformative when using unbiased estimators. This is why methods based on the mean square error in conjunction with the CRB are more relevant to evaluate resilience to multipath effects. The CRB establishes a theoretical limit on estimation performance by explicitly estimating the parameters of both the LOS signal and the multipath components signal. In the following subsections, we derive this bound based on the signal model introduced in (6), as it is sufficient to assess the robustness of signals against multipath. In addition, we introduce the estimators used to validate the CRB.

1. CRB Computation

The parameters to be estimated are collected in the following vector: $\bar{\boldsymbol{\epsilon}}^T = [\bar{\sigma}_n^2, \bar{\boldsymbol{\eta}}_0^T, \bar{\rho}_0, \bar{\phi}_0, \bar{\boldsymbol{\eta}}_1^T, \bar{\rho}_1, \bar{\phi}_1]$. From (6), we can write $\mathbf{x} \sim \mathcal{CN}\left(\mathbf{A}(\bar{\boldsymbol{\eta}}_0, \bar{\boldsymbol{\eta}}_1)\bar{\boldsymbol{\alpha}}, \bar{\sigma}_n^2 \mathbf{I}_N\right)$ and express the probability density function (pdf) as,

$$p_{\boldsymbol{\epsilon}}(\mathbf{x}, \bar{\boldsymbol{\epsilon}}) = \frac{1}{\left(\pi\bar{\sigma}_n^2\right)^N} e^{-\frac{1}{\bar{\sigma}_n^2}\|\mathbf{x}-\mathbf{A}(\bar{\boldsymbol{\eta}}_0,\bar{\boldsymbol{\eta}}_1)\bar{\boldsymbol{\alpha}}\|^2} . \tag{7}$$

The corresponding CRB for the estimation of $\bar{\boldsymbol{\epsilon}}$ is defined as the inverse of the Fisher Information Matrix (FIM) (Van Trees, 2001),

$$\mathbf{CRB}_{\boldsymbol{\epsilon}|\boldsymbol{\epsilon}} = \mathbf{F}_{\boldsymbol{\epsilon}|\boldsymbol{\epsilon}}^{-1}(\bar{\boldsymbol{\epsilon}}), \quad \mathbf{F}_{\boldsymbol{\epsilon}|\boldsymbol{\epsilon}}(\bar{\boldsymbol{\epsilon}}) = -E\left[\frac{\partial^2 \ln p(\mathbf{x}, \bar{\boldsymbol{\epsilon}})}{\partial\boldsymbol{\epsilon}\partial\boldsymbol{\epsilon}^T}\right] . \tag{8}$$

$$\mathbf{F}_{\boldsymbol{\epsilon}|\boldsymbol{\epsilon}}(\bar{\boldsymbol{\epsilon}}) = \begin{bmatrix} F_{\sigma_n^2|\boldsymbol{\epsilon}}(\bar{\boldsymbol{\epsilon}}) & \mathbf{0} & \mathbf{0} \\ \mathbf{0} & \mathbf{F}_{\boldsymbol{\theta}_0|\boldsymbol{\epsilon}}(\bar{\boldsymbol{\epsilon}}) & \mathbf{F}_{\boldsymbol{\theta}_0,\boldsymbol{\theta}_1|\boldsymbol{\epsilon}}(\bar{\boldsymbol{\epsilon}}) \\ \mathbf{0} & \mathbf{F}_{\boldsymbol{\theta}_1,\boldsymbol{\theta}_0|\boldsymbol{\epsilon}}(\bar{\boldsymbol{\epsilon}}) & \mathbf{F}_{\boldsymbol{\theta}_1|\boldsymbol{\epsilon}}(\bar{\boldsymbol{\epsilon}}) \end{bmatrix}, \tag{9}$$

where:

- $F_{\sigma_n^2|\boldsymbol{\epsilon}}(\bar{\boldsymbol{\epsilon}}) = N/\sigma_n^4$ (Lubeigt et al., 2020).
- $\mathbf{F}_{\boldsymbol{\theta}_0|\boldsymbol{\epsilon}}(\bar{\boldsymbol{\epsilon}})$ and $\mathbf{F}_{\boldsymbol{\theta}_1|\boldsymbol{\epsilon}}(\bar{\boldsymbol{\epsilon}})$ correspond to the FIMs of the LOS signal and its multipath when they are completely decoupled. These matrices have been derived and studied in (Medina et al., 2020) and (Das et al., 2020) for the general Gaussian Conditional Signal Model (CSM), including delay estimation and Doppler frequency estimation. The main results in (Medina et al., 2020) and (Das et al., 2020) regarding the single source CSM FIM terms are summarized in Section III.2.
- $\mathbf{F}_{\boldsymbol{\theta}_0,\boldsymbol{\theta}_1|\boldsymbol{\epsilon}}(\bar{\boldsymbol{\epsilon}}) = \mathbf{F}_{\boldsymbol{\theta}_1,\boldsymbol{\theta}_0|\boldsymbol{\epsilon}}(\bar{\boldsymbol{\epsilon}})^T$ characterizes the interference between both signals, that is, the influence of the multipath component on the estimations of the LOS parameter and inversely. The derivation of the FIM components is given in Section III.3.

2. Decoupled Fisher Information Matrix Terms

The two last diagonal blocks of the FIM given in equation (9) were derived for the single-source CSM case in (Medina et al., 2020). The main results are summarized here:

$$\mathbf{F}_{\boldsymbol{\theta}_i|\boldsymbol{\epsilon}}(\bar{\boldsymbol{\epsilon}}) = \frac{2f_s}{\sigma_n^2}\Re\left\{\mathbf{Q}_i\mathbf{W}\mathbf{Q}_i^H\right\} , \tag{10}$$

where $\mathbf{Q}_i,\ i \in \{1, 2\}$ and $\mathbf{W}$, defined in (Lubeigt et al., 2020), are reminded here under:

$$\mathbf{W} = \begin{bmatrix} w_1 & w_2^* & w_3^* \\ w_2 & W_{2,2} & w_4^* \\ w_3 & w_4 & W_{3,3} \end{bmatrix} \tag{11}$$

$$\mathbf{Q_i} = \begin{bmatrix} j\bar{\rho}_i\omega_c\bar{b}_i & 0 & -\bar{\rho}_i \\ 0 & -j\bar{\rho}_i\omega_c & 0 \\ 1 & 0 & 0 \\ j\bar{\rho}_i & 0 & 0 \end{bmatrix} \tag{12}$$

with the easy-to-use formulation w.r.t. the baseband signal samples:

$$w_1 = \frac{1}{f_s}\mathbf{s}^H\mathbf{s},\ w_2 = \frac{1}{f_s^2}\mathbf{s}^H\mathbf{D}\mathbf{s},\ w_3 = \mathbf{s}^H\mathbf{V}^{\Delta,1}(0)\mathbf{s},\ w_4 = \frac{1}{f_s}\mathbf{s}^H\mathbf{D}\mathbf{V}^{\Delta,1}(0)\mathbf{s},$$
$$W_{2,2} = \frac{1}{f_s^3}\mathbf{s}^H\mathbf{D}^2\mathbf{s},\ W_{3,3} = f_s\mathbf{s}^H\mathbf{V}^{\Delta,2}(0)\mathbf{s}, \tag{13}$$

where $\mathbf{s}$ is the baseband sample vector, $\mathbf{D}$ is defined in (46), $\mathbf{V}^{\Delta,1}$ in (48) and $\mathbf{V}^{\Delta,2}$ in (49).

The inversion of (10) suggested in (Medina et al., 2020) leads to a closed-form CRB expression of the time-delay, Doppler, phase, and amplitude parameters under the assumption of no multipath. Moreover, a notable feature is that the CRBs are expressed w.r.t. the baseband signal samples. Such CRBs were studied for different GNSS signals in (Das et al., 2020) and (Ortega et al., 2020).

3. Interference Fisher Information Matrix Terms

From the Slepian-Bangs formula (Kay, 1993; Ottersten et al., 1993), the non-diagonal blocks of the FIM, referred to as interference Fisher information matrices, are expressed as follows:

$$\mathbf{F}_{\boldsymbol{\theta}_1,\boldsymbol{\theta}_0|\boldsymbol{\epsilon}}(\bar{\boldsymbol{\epsilon}}) = \frac{2f_s}{\bar{\sigma}_n^2}\Re\left\{\mathbf{Q}_1\mathbf{W}^{\Delta}\mathbf{Q}_0^H\right\}\ , \tag{14}$$

where $\mathbf{Q}_0$, $\mathbf{Q}_1$ are defined in (Lubeigt et al., 2020, Appendix A.2), and $\mathbf{W}^{\Delta}$ is defined as

$$\mathbf{W}^{\Delta} = \begin{bmatrix} W_{1,1}^{\Delta} & W_{1,2}^{\Delta} & W_{1,3}^{\Delta} \\ W_{2,1}^{\Delta} & W_{2,2}^{\Delta} & W_{2,3}^{\Delta} \\ W_{3,1}^{\Delta} & W_{3,2}^{\Delta} & W_{3,3}^{\Delta} \end{bmatrix} e^{j\Delta\bar{\psi}}e^{-j\omega_c\Delta\bar{b}\bar{\tau}_0}\ , \tag{15}$$

where $\Delta\bar{b}$ and $\Delta\bar{\psi}$ are defined in (16)

$$\Delta\bar{\psi} = \bar{\psi}_1 - \bar{\psi}_0 = \Delta\bar{\phi} + \omega_c(\bar{b}_1\bar{\tau}_1 - \bar{b}_0\bar{\tau}_0),\ \Delta\bar{b} = \bar{b}_1 - \bar{b}_0,\ \Delta\bar{\phi} = \bar{\phi}_1 - \bar{\phi}_0 \tag{16}$$

and with the different components of the matrix $\mathbf{W}^{\Delta}$ expressed w.r.t the baseband signal samples given by

$$W_{1,1}^{\Delta} = \frac{1}{f_s}\mathbf{s}^H\mathbf{U}(\Delta\bar{b})\mathbf{V}^{\Delta,0}\left(\frac{\Delta\bar{\tau}}{T_s}\right)\mathbf{s}\ , \qquad W_{1,2}^{\Delta} = \frac{1}{f_s^2}\mathbf{s}^H\mathbf{D}\mathbf{U}(\Delta\bar{b})\mathbf{V}^{\Delta,0}\left(\frac{\Delta\bar{\tau}}{T_s}\right)\mathbf{s}\ , \tag{17}$$

$$W_{1,3}^{\Delta} = -\mathbf{s}^H\mathbf{U}(\Delta\bar{b})\mathbf{V}^{\Delta,1}\left(\frac{\Delta\bar{\tau}}{T_s}\right)\mathbf{s} + \frac{j\omega_c\Delta\bar{b}}{f_s}\mathbf{s}^H\mathbf{U}(\Delta\bar{b})\mathbf{V}^{\Delta,0}\mathbf{s}\ , \tag{18}$$

$$W_{2,1}^{\Delta} = \frac{1}{f_s^2}\mathbf{s}^H\mathbf{U}(\Delta\bar{b})\mathbf{V}^{\Delta,0}\left(\frac{\Delta\bar{\tau}}{T_s}\right)\mathbf{D}\mathbf{s}\ , \qquad W_{2,2}^{\Delta} = \frac{1}{f_s^3}\mathbf{s}^H\mathbf{D}\mathbf{U}(\Delta\bar{b}), \tag{19}$$

$$W_{2,3}^{\Delta} = -\frac{1}{f_s}\mathbf{s}^H\mathbf{U}(\Delta\bar{b})\mathbf{V}^{\Delta,1}\left(\frac{\Delta\bar{\tau}}{T_s}\right)\mathbf{D}\mathbf{s} + \frac{j\omega_c\Delta\bar{b}}{f_s^2}\mathbf{s}^H\mathbf{U}(\Delta\bar{b})\mathbf{V}^{\Delta,0}\left(\frac{\Delta\bar{\tau}}{T_s}\right)\mathbf{D}\mathbf{s}\ , \tag{20}$$

$$W_{3,1}^{\Delta} = \mathbf{s}^H\mathbf{U}(\Delta\bar{b})\mathbf{V}^{\Delta,1}\left(\frac{\Delta\bar{\tau}}{T_s}\right)\mathbf{s}\ , \qquad W_{3,2}^{\Delta} = \frac{1}{f_s}\mathbf{s}^H\mathbf{D}\mathbf{U}(\Delta\bar{b})\mathbf{V}^{\Delta,1}\left(\frac{\Delta\bar{\tau}}{T_s}\right)\mathbf{s}\ , \tag{21}$$

$$W_{3,3}^{\Delta} = f_s\mathbf{s}^H\mathbf{U}\left(\Delta\bar{b}\right)\mathbf{V}^{\Delta,2}\left(\frac{\Delta\bar{\tau}}{T_s}\right)\mathbf{s} + j\omega_c\Delta\bar{b}\mathbf{s}^H\mathbf{U}(\Delta\bar{b})\mathbf{V}^{\Delta,1}\left(\frac{\Delta\bar{\tau}}{T_s}\right)\mathbf{s}\ , \tag{22}$$

with $\mathbf{U}$ defined in (45) and $\mathbf{V}^{\Delta,0}$ defined in (47).

4. Dual-source estimators

a) Dual Source Conditional Maximum Likelihood Estimator

From the dual source CSM (6) and its pdf (7), the estimator $\widehat{\boldsymbol{\epsilon}}$ for the amplitude and the phase that maximize the likelihood is such that $(\widehat{\boldsymbol{\eta}_0}, \widehat{\boldsymbol{\eta}_1})$ maximizes the projection of the received signal into the subspace defined by the span matrix $\mathbf{A}$ (Ottersten et al.,

1993). As a consequence, the estimated parameters $(\widehat{\rho_0}, \widehat{\rho_1}, \widehat{\phi_0}, \widehat{\phi_1})$ directly depend on the time-delay and Doppler estimation. Finally, $\widehat{\sigma_n^2}$ is the orthogonal projection value:

$$(\widehat{\boldsymbol{\eta}_0}, \widehat{\boldsymbol{\eta}_1}) = \arg \max_{\boldsymbol{\eta}_0, \boldsymbol{\eta}_1} \left\| \mathbf{P}_{\mathbf{A}(\boldsymbol{\eta}_0, \boldsymbol{\eta}_1)} \mathbf{x} \right\|^2 \tag{23a}$$

$$\widehat{\rho_i} = \left| \left[\left(\mathbf{A}^H(\widehat{\boldsymbol{\eta}_0}, \widehat{\boldsymbol{\eta}_1}) \mathbf{A}(\widehat{\boldsymbol{\eta}_0}, \widehat{\boldsymbol{\eta}_1}) \right)^{-1} \mathbf{A}^H(\widehat{\boldsymbol{\eta}_0}, \widehat{\boldsymbol{\eta}_1}) \mathbf{x} \right]_i \right| \tag{23b}$$

$$\widehat{\phi_i} = \arg \left\{ \left[\left(\mathbf{A}^H(\widehat{\boldsymbol{\eta}_0}, \widehat{\boldsymbol{\eta}_1}) \mathbf{A}(\widehat{\boldsymbol{\eta}_0}, \widehat{\boldsymbol{\eta}_1}) \right)^{-1} \mathbf{A}^H(\widehat{\boldsymbol{\eta}_0}, \widehat{\boldsymbol{\eta}_1}) \mathbf{x} \right]_i \right\} \tag{23c}$$

$$\widehat{\sigma_n^2} = \frac{1}{N} \left\| \mathbf{P}^{\perp}_{\mathbf{A}(\boldsymbol{\eta}_0, \boldsymbol{\eta}_1)} \mathbf{x} \right\|^2 \tag{23d}$$

with the orthogonal projector of the span matrix A defined as $\mathbf{P}_{\mathbf{A}} = \mathbf{A} \left(\mathbf{A}^H \mathbf{A} \right)^{-1} \mathbf{A}^H$ and its complement defined as $\mathbf{P}^{\perp}_{\mathbf{A}} = \mathbf{I} - \mathbf{P}_{\mathbf{A}}$. Although this estimator is known to be computationally complex, it is also known to be asymptotically efficient (e.g., in the high-SNR regime (Renaux et al., 2006) for dual-source Gaussian CSM. This property makes it a powerful tool for validating previously derived CRBs.

b) Sub-optimal Estimator: CLEAN-RELAX

To mitigate the high computational cost of the CMLE, alternative estimators can be considered. Following the approach in (Lubeigt et al., 2020), this article implements a relaxed version of the CLEAN Relax Estimator (CRE) (Li and Stoica, 1996). This estimator operates under the assumption that the two signals are decoupled. The method begins by estimating the parameters $(\widehat{\tau_0}, \widehat{b_0}, \widehat{\rho_0}, \widehat{\phi_0})$ of the strongest signal using the cross-correlation function. The estimated signal is then subtracted from the received input, allowing the parameters $(\widehat{\tau_1}, \widehat{b_1}, \widehat{\rho_1}, \widehat{\phi_1})$ of the secondary signal to be estimated. These two steps are iterated until the parameters converge. This method is specifically designed for scenarios that involve two signals. In GNSS applications, a similar approach is known as the Multipath Estimating Delay Lock Loop (MEDLL), widely used for multipath mitigation (Townsend et al., 1995). The CRE is considered a suboptimal estimator as its validity depends on certain conditions. In particular, the decoupling assumption holds when the time difference $\Delta\bar{\tau}$ is large enough relative to the sharpness of the cross-correlation function. When signals are closely spaced, this estimator may not perform well. However, when the signals are clearly separated, the CRE behaves asymptotically as the CMLE.

IV. MULTIPATH PERFORMANCE ESTIMATION UNDER MISSPECIFIED SIGNAL MODEL

Unfortunately, in standard receivers, implementing estimators that account for multipath signals is often impractical due to their complexity or simply because the receiver is unaware of potential signal reflections. This inherent simplification results in *model misspecification*, leading to a degradation of performance in estimating the synchronization parameters. To quantify this performance loss, we created a reduced (and misspecified) version of the signal model. Therefore, the discrete signal vector of the misspecified model can be defined as

$$\mathbf{x} = \rho e^{j\phi} \mathbf{a}(\boldsymbol{\eta}) + \mathbf{w}, \ \mathbf{w} \sim \mathcal{CN}(0, \bar{\sigma}_n^2 \mathbf{I}_N) \ , \tag{24}$$

The misspecified signal parameters can be cast in a vector $\boldsymbol{\eta} = (\tau, b)^\top \in \mathbb{R}^2$ and the complete set of unknown misspecified parameters is $\boldsymbol{\Phi}^\top = (\sigma_n^2, \boldsymbol{\eta}^\top, \rho, \phi) = (\sigma_n^2, \boldsymbol{\theta}^\top) \in \Psi \subset \mathbb{R}^+ \times \mathbb{R}^2 \times \mathbb{R}^+ \times [0, 2\pi]$. Moreover, we define $\mathbf{a}(\boldsymbol{\eta})^T = \left(\dots, \ s(nT_s - \tau) e^{-j\omega_c b(nT_s - \tau)}, \ \dots \right)$ and $\alpha = \rho e^{j\phi}$. By collecting the previous definitions, the Gaussian-based, *multipath-unaware* statistical model for the observation vector in (24) can be expressed as:

$$\mathcal{F}_{\boldsymbol{\Phi}} \triangleq \left\{ f_{\boldsymbol{\Phi}} | f_{\mathbf{x}}(\mathbf{x}; \boldsymbol{\Phi}) = \mathcal{CN}(\alpha \boldsymbol{\mu}(\boldsymbol{\eta}), \sigma_n^2 \boldsymbol{I}_N); \boldsymbol{\Phi} \in \Psi \right\} . \tag{25}$$

Since in general $p_{\bar{\epsilon}} \notin \mathcal{F}_{\boldsymbol{\Phi}}$ no estimator can accurately recover the true parameter vector $\bar{\epsilon}$. The best achievable estimate is the so-called *pseudotrue* parameter vector $\boldsymbol{\Phi}_{pt} \in \Psi$ (Fortunati et al., 2018, 2017), which minimizes the Kullback-Leibler divergence (KLD). Specifically, it is the vector that minimizes the divergence $\{D(p_{\bar{\boldsymbol{\epsilon}}} \| f_{\boldsymbol{\Phi}})\}$. Therefore, $\boldsymbol{\Phi}_{pt}$ yields to

$$\boldsymbol{\epsilon}_{pt} = \arg \min_{\boldsymbol{\Phi} \in \Psi} \{D(p_{\bar{\boldsymbol{\epsilon}}} \| f_{\boldsymbol{\Phi}})\} = \arg \min_{\boldsymbol{\epsilon}} \{E_{p_{\bar{\boldsymbol{\epsilon}}}} [-\ln f_{\mathbf{x}}(\mathbf{x}; \boldsymbol{\Phi})]\}. \tag{26}$$

where $E_{p_\epsilon}[\cdot]$ is the expectation with respect to the true probability density function. Following (Fortunati and Ortega, 2024), the pseudotrue parameter vector $\boldsymbol{\theta}_{pt}^T = \left[\boldsymbol{\eta}_{pt}^T, \rho_{pt}, \phi_{pt}\right]$ yields to

$$\boldsymbol{\theta}_{pt} = \arg\ \min_{\boldsymbol{\theta}}\{\|\mathbf{A}(\bar{\boldsymbol{\eta}}_0, \bar{\boldsymbol{\eta}}_1)\bar{\boldsymbol{\alpha}} - \alpha\mathbf{a}(\boldsymbol{\eta})\|^2\}. \tag{27}$$

In the context of this misspecified model, the misspecified CMLE acts as a single-source ML estimator aimed at estimating the pseudotrue parameter vector $\boldsymbol{\theta}_{pt}$ and it can be shown (Fortunati et al., 2017) that it is consistent and asymptotically efficient, where the efficiency is measured by the misspecified CRB.

After establishing the set of pseudotrue parameters, the MCRB is expressed as a combination of two information matrices (Fortunati et al., 2017): $\mathbf{A}(\boldsymbol{\theta}_{pt})$ corresponding to the misspecification of the model and $\mathbf{B}(\boldsymbol{\theta}_{pt})$ corresponding to the FIM of a single source CSM.

$$\mathbf{MCRB}(\boldsymbol{\theta}_{pt}) = \mathbf{A}(\boldsymbol{\theta}_{pt})^{-1}\mathbf{B}(\boldsymbol{\theta}_{pt})\mathbf{A}(\boldsymbol{\theta}_{pt})^{-1} \tag{28}$$

$$[\mathbf{A}(\boldsymbol{\theta}_{pt})]_{p,q} = \frac{2}{\sigma_n^2}\Re\left\{(\delta\mathbf{a})^H\left(\frac{\partial^2\alpha_{pt}\mathbf{a}_{pt}}{\partial\theta_p\partial\theta_q}\right)\right\}\Bigg|_{\boldsymbol{\theta}=\boldsymbol{\theta}_{pt}} - [\mathbf{B}(\boldsymbol{\theta}_{pt})]_{p,q} \tag{29}$$

$$[\mathbf{B}(\boldsymbol{\theta}_{pt})]_{p,q} = \frac{2}{\sigma_n^2}\Re\left\{\left(\frac{\partial\alpha_{pt}\mathbf{a}_{pt}}{\partial\theta_p}\right)^H\left(\frac{\partial\alpha_{pt}\mathbf{a}_{pt}}{\partial\theta_q}\right)\right\}\Bigg|_{\boldsymbol{\theta}=\boldsymbol{\theta}_{pt}} \tag{30}$$

with $\delta\mathbf{a} \triangleq \bar{\alpha}_0\mathbf{a}_0 + \bar{\alpha}_1\mathbf{a}_1 - \alpha_{pt}\mathbf{a}_{pt}$ the difference of the means between the true and misspecified models. Following the results of (Medina et al., 2020) and under the assumption of the band-limited signal, a closed-form expression of $\mathbf{B}(\boldsymbol{\theta}_{pt})$ is given by:

$$\mathbf{B}(\boldsymbol{\theta}_{pt}) = \frac{2f_s}{\sigma_n^2}\Re\{\mathbf{Q}_{pt}\mathbf{W}\mathbf{Q}_{pt}^H\} \tag{31}$$

where $\mathbf{W}$ is defined in (11) and

$$\mathbf{Q}_{pt} = \begin{bmatrix} j\rho_{pt}\omega_c b_{pt} & 0 & -\rho_{pt} \\ 0 & -j\rho_{pt}\omega_c & 0 \\ 1 & 0 & 0 \\ j\rho_{pt} & 0 & 0 \end{bmatrix} \tag{32}$$

The closed-form expression of $\mathbf{A}(\boldsymbol{\theta}_{pt})$ is given by:

$$[\mathbf{A}(\boldsymbol{\theta}_{pt})]_{p,q} = \frac{2f_s}{\sigma_n^2}\Re\{[\mathbf{Q}_q]_{p,\cdot}\,\mathbf{W}^{\mathbf{A}}\} - [\mathbf{B}(\boldsymbol{\theta}_{pt})]_{p,q} \tag{33}$$

where $\mathbf{W}^{\mathbf{A}} = \bar{\alpha}_0\mathbf{w}^{\mathbf{A}}(\bar{\boldsymbol{\eta}}_0) + \bar{\alpha}_1\mathbf{w}^{\mathbf{A}}(\bar{\boldsymbol{\eta}}_1) - \alpha_{pt}\mathbf{w}^{\mathbf{A}}(\boldsymbol{\eta}_{\boldsymbol{pt}})$, for $k \in \{0, 1, pt\},\ \Delta\tau_k = \bar{\tau}_k - \tau_{pt},\ \Delta b_k = \bar{b}_k - b_{pt}$ and $\mathbf{w}^{\mathbf{A}}(\boldsymbol{\eta}_k)$ is a six-element vector:

$$\mathbf{w}_1^{\mathbf{A}}(\boldsymbol{\eta}_k)^* = \frac{1}{f_s}\mathbf{s}^H\mathbf{U}\left(\frac{f_c\Delta b_k}{f_s}\right)\mathbf{V}^{\Delta,0}\left(\frac{\Delta\tau_k}{T_s}\right)\mathbf{s}\, e^{j\omega_c b_k\Delta\tau_k}, \tag{34}$$

$$\mathbf{w}_2^{\mathbf{A}}(\boldsymbol{\eta}_k)^* = \frac{1}{f_s^2}\mathbf{s}^H\mathbf{D}\mathbf{U}\left(\frac{f_c\Delta b_k}{f_s}\right)\mathbf{V}^{\Delta,0}\left(\frac{\Delta\tau_k}{T_s}\right)\mathbf{s}\, e^{j\omega_c b_k\Delta\tau_k}, \tag{35}$$

$$\mathbf{w}_3^{\mathbf{A}}(\boldsymbol{\eta}_k)^* = \frac{1}{f_s^3}\mathbf{s}^H\mathbf{D}^2\mathbf{U}\left(\frac{f_c\Delta b_k}{f_s}\right)\mathbf{V}^{\Delta,0}\left(\frac{\Delta\tau_k}{T_s}\right)\mathbf{s}\, e^{j\omega_c b_k\Delta\tau_k}, \tag{36}$$

$$\mathbf{w}_4^{\mathbf{A}}(\boldsymbol{\eta}_k)^* = \left(-\mathbf{s}^H\mathbf{U}\left(\frac{f_c\Delta b_k}{f_s}\right)\mathbf{V}^{\Delta,1}\left(\frac{\Delta\tau_k}{T_s}\right)\mathbf{s} + \frac{j\omega_c\Delta b_k}{f_s}\mathbf{s}^H\mathbf{U}\left(\frac{f_c\Delta b_k}{f_s}\right)\mathbf{V}^{\Delta,0}\left(\frac{\Delta\tau_k}{T_s}\right)\mathbf{s}\right) e^{j\omega_c b_k\Delta\tau_k}, \tag{37}$$

$$\begin{aligned}\mathbf{w}_5^{\mathbf{A}}(\boldsymbol{\eta}_k)^* = \Bigg(&-\frac{1}{f_s}\mathbf{s}^H\mathbf{U}\left(\frac{f_c\Delta b_k}{f_s}\right)\mathbf{V}^{\Delta,0}\left(\frac{\Delta\tau_k}{T_s}\right)\mathbf{s} - \frac{1}{f_s}\mathbf{s}^H\mathbf{D}\mathbf{U}\left(\frac{f_c\Delta b_k}{f_s}\right)\mathbf{V}^{\Delta,1}\left(\frac{\Delta\tau_k}{T_s}\right)\mathbf{s}\\ &+j\frac{\omega_c\Delta b_k}{f_s^2}\mathbf{s}^H\mathbf{D}\mathbf{U}\left(\frac{f_c\Delta b_k}{f_s}\right)\mathbf{V}^{\Delta,0}\left(\frac{\Delta\tau_k}{T_s}\right)\mathbf{s}\Bigg) e^{j\omega_c b_k\Delta\tau_k},\end{aligned} \tag{38}$$

$$\begin{aligned}\mathbf{w}_6^{\mathbf{A}}(\boldsymbol{\eta}_k)^* = \Bigg(&-f_s\mathbf{s}^H\mathbf{U}\left(\frac{f_c\Delta b_k}{f_s}\right)\mathbf{V}^{\Delta,2}\left(\frac{\Delta\tau_k}{T_s}\right)\mathbf{s} - j2\omega_c\Delta b_k\mathbf{s}^H\mathbf{U}\left(\frac{f_c\Delta b_k}{f_s}\right)\mathbf{V}^{\Delta,1}\left(\frac{\Delta\tau_k}{T_s}\right)\mathbf{s}\\ &-\frac{(\omega_c\Delta b_k)^2}{f_s}\mathbf{s}^H\mathbf{U}\left(\frac{f_c\Delta b_k}{f_s}\right)\mathbf{V}^{\Delta,0}\left(\frac{\Delta\tau_k}{T_s}\right)\mathbf{s}\Bigg) e^{j\omega_c b_k\Delta\tau_k},\end{aligned} \tag{39}$$

and with $[\mathbf{Q}_q]_{p,:}$ being the p-th row of the $\mathbf{Q}_q$ matrix in $[\mathbf{Q}_1\ \mathbf{Q}_2\ \mathbf{Q}_3\ \mathbf{Q}_4]$ with the complete expression available in the appendix B, equation (51). The proof origin of the $\mathbf{Q}_q$ matrices can be found in (Lubeigt et al., 2023, Appendix A.2).

1. Mismatched Maximum Likelihood Estimator

After defining the misspecified model (24), the Mismatched Maximum Likelihood Estimator (MMLE) is a single-source MLE with the purpose of estimating the pseudotrue parameters (Ortega Espluga, 2025, Chapter 3).

$$\hat{\boldsymbol{\eta}} = \arg\max_{\boldsymbol{\eta}}\left\{\left|\left(\mathbf{a}^H(\boldsymbol{\eta})\mathbf{a}(\boldsymbol{\eta})\right)^{-1}\mathbf{a}^H(\boldsymbol{\eta})\mathbf{x}\right|^2\right\} \tag{40a}$$

$$\hat{\rho} = \left|\left(\mathbf{a}^H(\hat{\boldsymbol{\eta}})\mathbf{a}(\hat{\boldsymbol{\eta}})\right)^{-1}\mathbf{a}^H(\hat{\boldsymbol{\eta}})\mathbf{x}\right| \tag{40b}$$

$$\hat{\boldsymbol{\Phi}}(\hat{\boldsymbol{\eta}}) = \arg\left\{\left(\mathbf{a}^H(\hat{\boldsymbol{\eta}})\mathbf{a}(\hat{\boldsymbol{\eta}})\right)^{-1}\mathbf{a}^H(\hat{\boldsymbol{\eta}})\mathbf{x}\right\} \tag{40c}$$

where $\mathbf{x}$ is the received signal, correlated with a local replica $\mathbf{a}$. In the specific case of the MMLE, the local replica does not include any interferences. It is simply a nominal LOS signal.

V. SIMULATION PLAN

1. Sampling frequency and integration time selection

a) Sampling frequency selection

As can be seen in Table 1 and Figure 1, working with meta-signals significantly increases the signal bandwidth. So, to meet the Shannon-Nyquist criterion, the subcarrier frequency - expressing the spectral spread of the signal - must be considered. A basic application of the criterion would lead to $f_s \geq 2f_{sub}$. However, with respect to the algorithms implemented (CRE and MMLE) and in order to have good signal resolution, it is useful to aim for a higher sampling frequency such as $f_s = 8f_{sub}$. Thus, the sampling frequencies used in this paper are summarized in Table 2.

Signal	Shannon-Nyquist criterion	Used sampling frequency
GPS L1 C/A	2 MHz	8 MHz
Galileo E5	30 MHz	120 MHz
GPS L2-L5	50 MHz	200 MHz

Table 2: Signal plan sampling frequency

b) Integration time selection

Because of the conventional signals used in this article to build meta-signals, homogeneous coherent integration times have been chosen based on the most limiting PRN code. To have a complete GPS L2 CM code, a common integration of 20 ms must be chosen for all signals. Then the following PRN code durations and number of code periods have been applied:

- GPS L1 C/A: $T_{\mathrm{PRN}} = 1$ ms, $N_{\mathrm{PRN}} = 20$;
- Galileo E5: $T_{\mathrm{PRN}} = 1$ ms, $N_{\mathrm{PRN}} = 20$;
- GPS L2-L5: $T_{\mathrm{PRN}} = 20$ ms, $N_{\mathrm{PRN}} = 1$.

2. Limitation due to sampling frequency and integration time

As explained previously, exploiting GNSS meta-signals requires high sampling frequencies, over 100 MHz. This results in a high computing complexity, for signals with an integration time of 20 ms, which limits the possibility of simulations to run in a reasonable time. That is why, in this contribution, the simulations using the dual source conditional maximum likelihood estimator, introduced in Section III.4 a), are not presented. In (Lubeigt et al., 2020), this estimator was proven to be efficient for conventional GNSS signals when the CLEAN Relax estimator failed.

Furthermore, GPS L2-L5 meta-signal is presented only from a bound and misspecified scenario perspective. The amount of computing memory required to run simulations on dual-source estimators with this signal was too important and induced weeks of simulations on high-performance computers.

3. Simulation process

Before looking at the behavior of meta-signals in a harsh environment, a study of the single source CRB (1S-CRB), which is the Cramér-Rao Lower Bound of a signal without any kind of interference, would suggest a first interest in using meta-signals for precise positioning. Some of these results are already presented in the literature (Das et al., 2020) and recalled for the completeness of the contribution.

a) Single source Cramér-Rao Lower Bounds

First of all, from a single source perspective, meta-signals bring a new level of estimation performance. As shown in Figure 2, moving from GPS L1 C/A to a meta-signal such as Galileo E5 or GPS L2-L5 will reduce the error on the delay estimation from some meters to tens of centimeters. However, on the Doppler effect side, meta-signals do not ease the estimation. In fact, the precision of the Doppler effect estimation is mainly related to the integration time, which is 20 ms for all signals in this contribution.

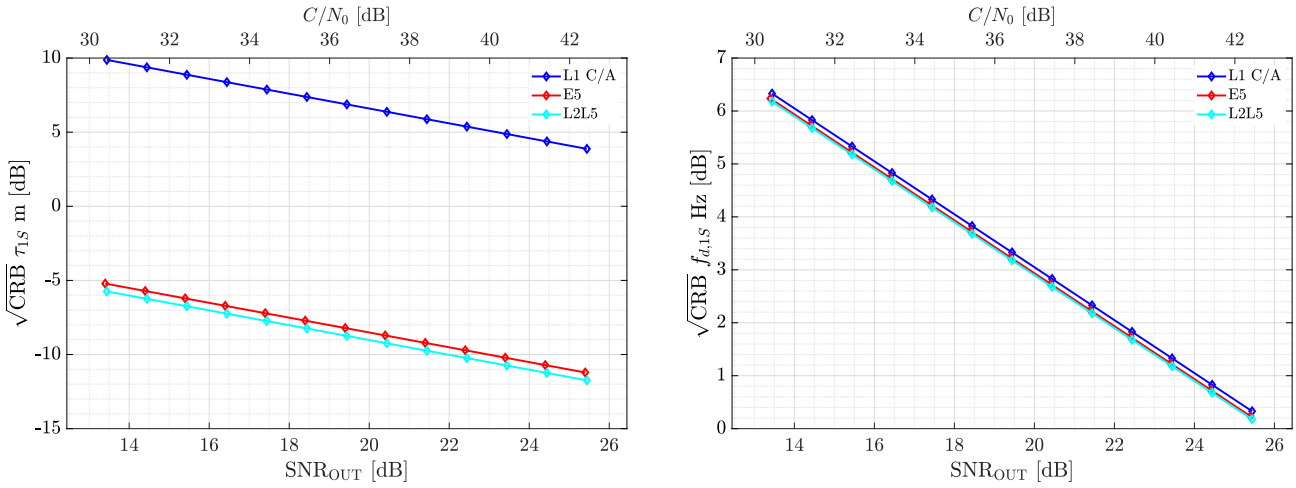

Figure 2: 1S-CRB on delay and Doppler effect estimation for all signals.

b) Multipath simulations

To assess the robustness of meta-signals in multipath situations, the Galileo E5 and GPS L2-L5 signals face different scenarios. The objective is to find relevant scenarios where an algorithm such as CLEAN Relax shows difficulties in mitigating the

multipath situation. This limit depends on the sampling frequency f_s (Lubeigt et al., 2020). Thus, for a standard GNSS receiver with a sampling frequency of around $4 - 8$ MHz, it corresponds to a delay between the LOS and NLOS signals of $73 - 37$ m. Moreover, the other interesting estimator to take into account is the misspecified maximum likelihood estimator. When dealing with this estimator, it is of interest to find a scenario in which the pseudotrue parameters defined in Section IV are different from the true parameters of the LOS signal. Thus, we look for a non-nominal scenario in the sense of multipath impact on the estimation of the pseudotrue and the true parameters. Solving numerically equation (41) in the neighborhood of the true parameters of the LOS signal gives the composition of the signals with the highest ambiguity for a given sampling frequency and signal-to-noise ratio.

$$(\bar{\tau}_1, \bar{b}_1)_1 = \max_{\Delta\bar{\tau}, \Delta\bar{b}} \left\{ \sqrt{\mathrm{MCRB}_\tau(\Delta\bar{\tau}, \Delta\bar{b}) + |\bar{\tau}_0 - \tau_{pt}|^2} \right\} \tag{41a}$$

$$(\bar{\tau}_1, \bar{b}_1)_2 = \max_{\Delta\bar{\tau}, \Delta\bar{b}} \left\{ \sqrt{\mathrm{MCRB}_b(\Delta\bar{\tau}, \Delta\bar{b}) + |\bar{b}_0 - b_{pt}|^2} \right\} \tag{41b}$$

With $\Delta\bar{\tau} = \bar{\tau}_1 - \bar{\tau}_0$ and $\Delta\bar{b} = \bar{b}_1 - \bar{b}_0$ the relative delay and Doppler between the LOS and NLOS signals. Solving equation (41) gives two possible scenarios. One affects mainly the delay estimation, $(\bar{\tau}_1, \bar{b}_1)_1$. The other one mainly affects the estimation of the Doppler effect, $(\bar{\tau}_1, \bar{b}_1)_1$. Accoring to the objectives of the simulations and implementations aspects, one scenario can be chosen.

For a better understanding of the physical values, the Doppler effect b, independent of the carrier frequency f_c, is now expressed through the Doppler frequency $f_d = b \cdot f_c$.

Thus, to assess the interest of using a meta-signal versus a conventional one, the simulations are performed with the following pattern:

- Validate the bounds and mean square errors with an unambiguous GPS L1 C / A simulation: $\Delta\bar{\tau} = 586$ m, $\Delta\bar{f}_d = 10$ Hz.
- Play a worst-case scenario where the CRE cannot properly mitigate the multipath on GPS L1 C / A: $\Delta\bar{\tau} = 37$ m, $\Delta\bar{f}_d = -4$ Hz.
- Run the latter on the first promising meta-signal: Galileo E5.
- Play a worst-case scenario where the CRE cannot efficiently mitigate the multipath on Galileo E5: $\Delta\bar{\tau} = 7$ m, $\Delta\bar{f}_d = -9.5$ Hz.
- Due to the computational resources required to run a CLEAN Relax estimator on the GPS L2-L5 meta-signal, only MCRB and its RMSE are studied to compare this signal with Galileo E5. The study of this single scenario is also supported by the proximity of the bounds between Galileo E5 and GPS L2-L5 in Figures 2 and 4.

Due to the relative position of the bounds in Figure 2, it could be assumed that GPS L2-L5 offers the best multipath robustness. This assumption can be supported by the thickness of the main peak of the autocorrelation function (ACF) in Figure 3. However, a question is raised about the involvement of secondary peaks in estimating signal parameters in the presence of noise.

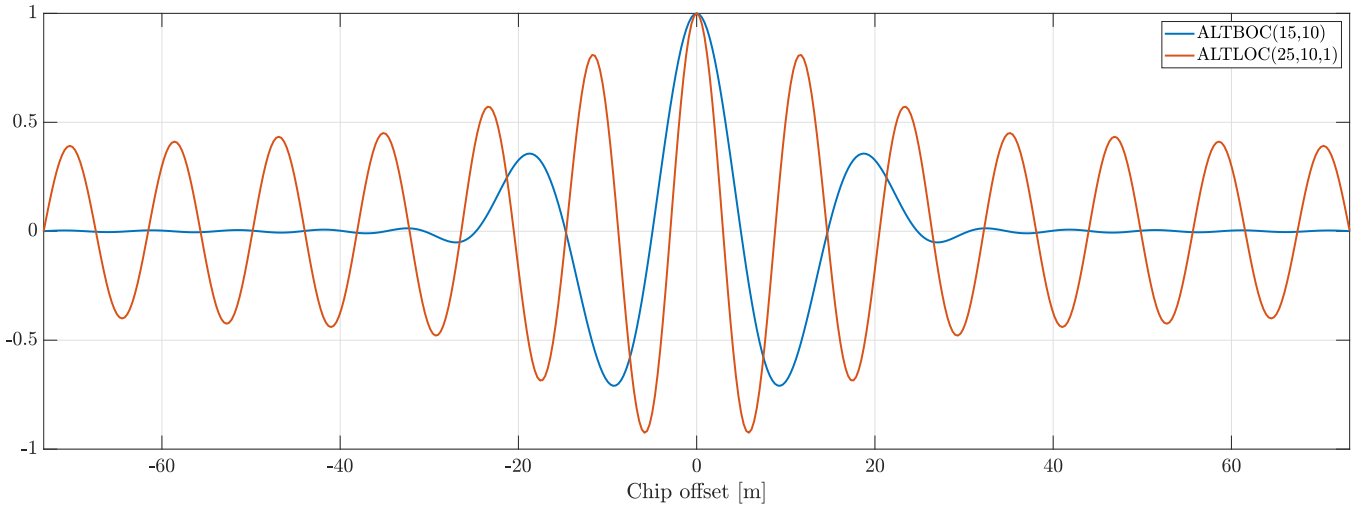

Figure 3: GPS L2C + L5 (red) and Galileo E5 (blue) autocorrelation functions

Table 3 summarizes all the bounds and estimators computed in this contribution.

	Signal	Estimator	Bound	$\Delta\bar{\tau}$ (m)	$\bar{\rho}_1/\bar{\rho}_0$	$\Delta\bar{\phi}$ (°)	$\bar{f}_{d0}/\bar{f}_{d1}$ (Hz)
(a)	GPS L1 C/A	CRE	2S-CRB	586	0.5	180	10/20
(b1)	GPS L1 C/A	CRE	2S-CRB	37	0.5	180	10/6
(b2)	GPS L1 C/A	MMLE	MCRB	37	0.5	180	10/6
(b3)	Galileo E5	CRE	2S-CRB	37	0.5	180	10/6
(c1)	Galileo E5	CRE	2S-CRB	7	0.5	180	10/0.5
(c2)	Galileo E5	MMLE	MCRB	7	0.5	180	10/0.5
(c3)	GPS L2-L5	MMLE	2S-CRB	7	0.5	180	10/0.5

Table 3: Simulation scenarios

The figures presented in Section VI, obtained through Monte Carlo simulation for different SNRs at the output of the correlators, plot the CRBs for delay and Doppler for the Line-of-Sight (LOS) signal and its multipath, as well as the Root Mean Square Error of the corresponding estimator. The SNR at the output of the correlator is given by (Ghizzo, 2025; Ortega Espluga, 2025):

$$\mathrm{SNR}_{\mathrm{OUT}} = \frac{C}{N_0} T_{\mathrm{PRN}} N_{\mathrm{PRN}} \tag{42}$$

where C/N_0 (Hz) is the carrier-to-noise density ratio, T_{PRN} is the duration of the PRN code period in seconds and N_{PRN} is the number of code periods processed for the estimation. Therefore, the coherent integration time is given by $T_I = T_{\mathrm{PRN}} N_{\mathrm{PRN}}$.

c) Implementation

Before presenting the results, it seems relevant to talk about some interesting aspects of the implementation of the CRE algorithm. Even if the CRE is less demanding than the CMLE, some optimization can still be performed in order to reduce the computation time of Monte-Carlo simulations from days to a couple of hours.

On the one hand, in the computation of the CRB, the oversampled vector representing the signal contains tens of thousands of points. However, it appears that the products $\mathbf{V}^{\Delta,0}\left(\frac{\Delta\bar{\tau}}{Ts}\right)\mathbf{s}$, $\mathbf{V}^{\Delta,0}\left(\frac{\Delta\bar{\tau}}{Ts}\right)\mathbf{Ds}$, $\mathbf{V}^{\Delta,1}\left(\frac{\Delta\bar{\tau}}{Ts}\right)\mathbf{s}$, $\mathbf{V}^{\Delta,1}\left(\frac{\Delta\bar{\tau}}{Ts}\right)\mathbf{Ds}$ and $\mathbf{V}^{\Delta,2}\left(\frac{\Delta\bar{\tau}}{Ts}\right)\mathbf{s}$ are linear convolutions of the vectors $\mathbf{s}$ and $\mathbf{Ds}$ by the vectors $\mathbf{V}^{\Delta,i}$, $i \in \{0,1,2\}$. Thanks to the zero padding operation, the circular and linear convolution can be linked. That is why, by computing a circular convolution thanks to the Fast Fourier Transform and a zero padding large enough (twice the size of the signal vector), the linear convolution can be approximated as a portion of the circular one. Thus, the previously defined products are extracted from the circular convolution.

On the other hand, an optimization can be performed by dynamically sizing the Doppler frequency search space. It is known that the error of the MLE asymptotically follows a centered normal distribution with variance equal to the CRB. Then, for each SNR, the frequency window can be constrained between

$$\min(\bar{f}_{d0} - 3\sqrt{\mathrm{CRB}_{b0}} \cdot f_c,\ \bar{f}_{d1} - 3\sqrt{\mathrm{CRB}_{b1}} \cdot f_c)$$

and

$$\max(\bar{f}_{d0} + 3\sqrt{\mathrm{CRB}_{b0}} \cdot f_c,\ \bar{f}_{d1} + 3\sqrt{\mathrm{CRB}_{b1}} \cdot f_c)$$

with f_c the signal carrier frequency, $\bar{f}_{d0}$ and $\bar{f}_{d1}$, respectively, the Doppler frequencies for the LOS signal and the multipath.

VI. RESULTS AND DISCUSSION

1. Theoretical prediction of meta-signal estimation performances in presence of multipath

To introduce this section, a global overview of the estimation bounds for the LOS parameters and the associated MCRB is suggested. Figure 4 is computed using the limit scenario of GPS L1 C/A: $\Delta\bar{\tau} = 37$ m and $\Delta\bar{f}_d = -4$ Hz. A first observation confirms the idea of using meta-signals versus conventional signals such as GPS L1 C/A to increase the robustness against multipaths. When a mitigation method is applied, a gain of 18 dB can be expected in the estimation of the true delay of the LOS signal ($\bar{\tau}_0$). Although 1S-CRB, Figure 2 does not show any improvement in the estimation of Doppler frequency. From a multipath mitigation and robustness point of view, the results are now in favor of the meta-signals with a gain of 3 dB with respect to the scenario used. The second observation concerns the relative position of the GPS L2-L5 CRB applied to the estimation of $\bar{\tau}_0$ with respect to that of Galileo E5. Even if the ACF of GPS L2-L5 offers a sharper main peak, its CRB is above the one of Galileo E5, showing a counterintuitive point that the Galileo E5 can perform better than GPS L2-L5 in some scenarios.

The third observation is about biased MCRB. In this scenario, Galileo E5 seems to be the most promising signal with a misspecified biased bound that overlaps the dual source bound for the estimation of $\bar{\tau}_0$ and $\bar{b}_0$. When using GPS L2-L5 in this context, a standard receiver will suffer a loss around 5 to 7 dB in the high SNR regime for the delay estimation and about 1 dB for the Doppler effect estimation.

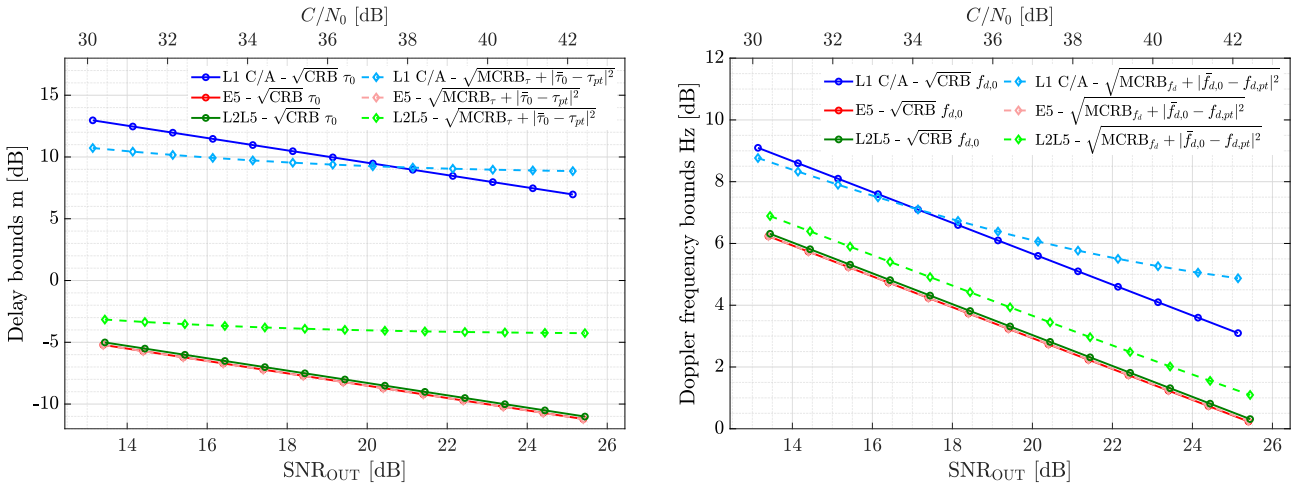

Figure 4: CRB of the LOS signal parameters and MCRB with bias on delay and Doppler effect estimation for all signals.

2. Limitation of multipath mitigation on GPS L1 C/A

	Signal	Estimator	Bound	$\Delta\bar{\tau}$ (m)	$\bar{\rho}_1/\bar{\rho}_0$	$\Delta\bar{\phi}$ (°)	$\bar{f}_{d0}/\bar{f}_{d1}$ (Hz)
(a)	GPS L1 C/A	CRE	2S-CRB	586	0.5	180	10/20
(b1)	GPS L1 C/A	CRE	2S-CRB	37	0.5	180	10/6

Table 4: Simulation scenarios for GPS L1 C/A

In scenario (a) from Table 4, the LOS signal and the multipath are clearly separated with a path difference of 586 m (2 GPS L1 C/A code chips). Figure 5 presents the CRE performances with application to the conventional GPS L1 C / A signal. The results presented in (Lubeigt et al., 2020), along with the convergence region around $\mathrm{SNR}_{\mathrm{OUT}} = 21$ dB for the estimation of the delay of the NLOS signal, confirmed this simulation as a reference for the following of this contribution. The convergence region represents the SNR regime, where the CRE can successfully estimate the LOS signal and then the NLOS signal. For a given signal, this region is mainly affected by the multipath configuration. A more ambiguous multipath results in the latter convergences to the CRB, until a limit is reached in the capacity of the CRE at estimating the signal parameters.

With GPS L1 C/A this limit is reached with a separation of 37 m. In Figure 6 a plateau appears at high SNRs after a latter convergence of the mean square error of the estimator. The estimation of the Doppler effect also presents difficulties in convergence to the CRB with a plateau as well in the high-SNR region. The estimator is then no longer efficient in the high-SNR regime.

From a misspecified receiver point of view, the estimate of delay and Doppler effect is biased because the estimation converges to the pseudotrue parameters. Figure 7 shows a non-null bias for both delay and Doppler. This bias is limiting the performances of the single source MLE when trying to estimate the true parameter with a precision around 10 m. However, in a receiver, the maximum likelihood estimator will be efficient to converge to the pseudotrue parameter.

3. Application to Galileo E5

When applying the latter scenario (b1) ($\Delta\bar{\tau} = 37$ m and $\Delta\bar{f}_d = -4$ Hz) to Galileo E5 (b3), Figure 8 shows that the CRE can now again clearly identify the signal components. It is interesting to note that the convergence to the CRB appears in the same $\mathrm{SNR}_{\mathrm{OUT}}$ region, between 16 dB and 22 dB. Moreover, a precision of 22 cm is reached in the estimation of the delay of the LOS signals at $\mathrm{SNR}_{\mathrm{OUT}} = 16$ dB, while GPS L1 C/A could only offer a 6 m-accuracy for the same $\mathrm{SNR}_{\mathrm{OUT}}$ when the signals were separated by 586 m.

However, when increasing the ambiguity between the LOS and NLOS signals by decreasing the separation between the LOS

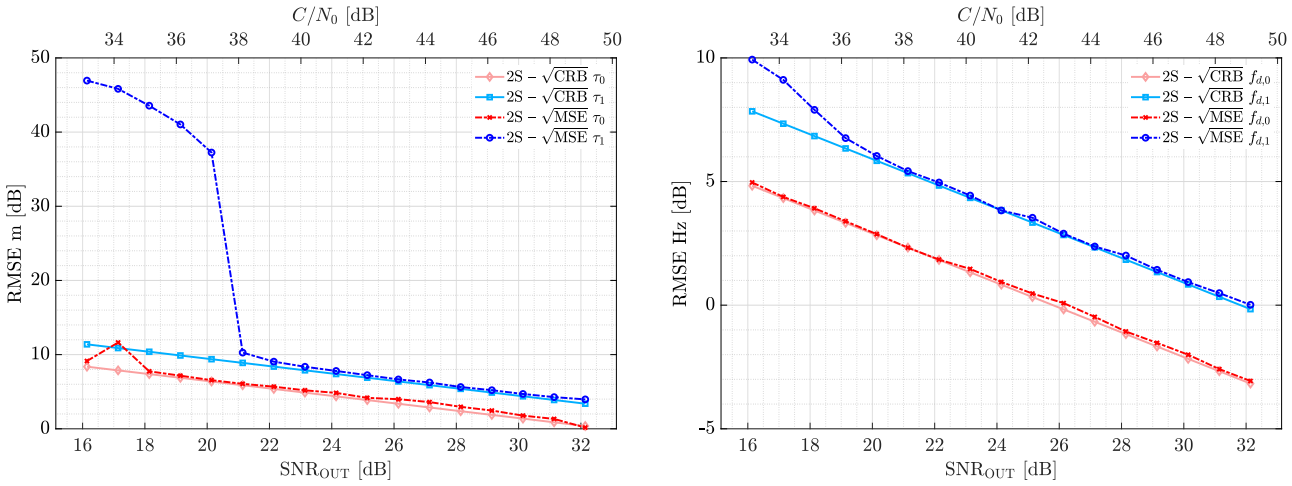

Figure 5: (a) CRE mean square error for delay (left) and Doppler effect (right) with $\Delta\tau = 586$ m on GPS L1 C/A.

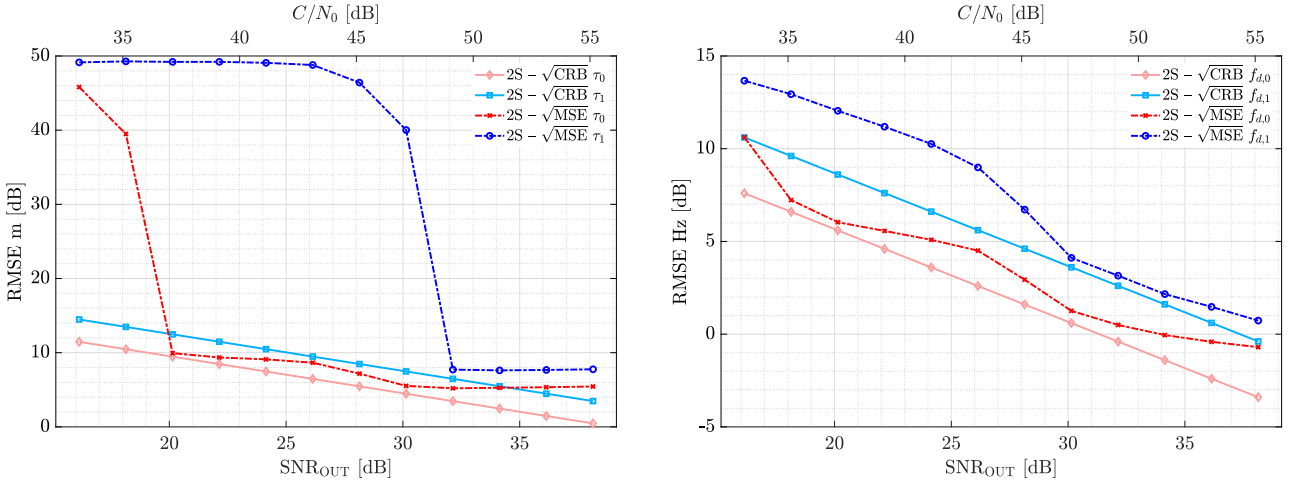

Figure 6: (b1) CRE mean square error for delay (left) and Doppler effect (right) with $\Delta\tau = 37$ m on GPS L1 C/A.

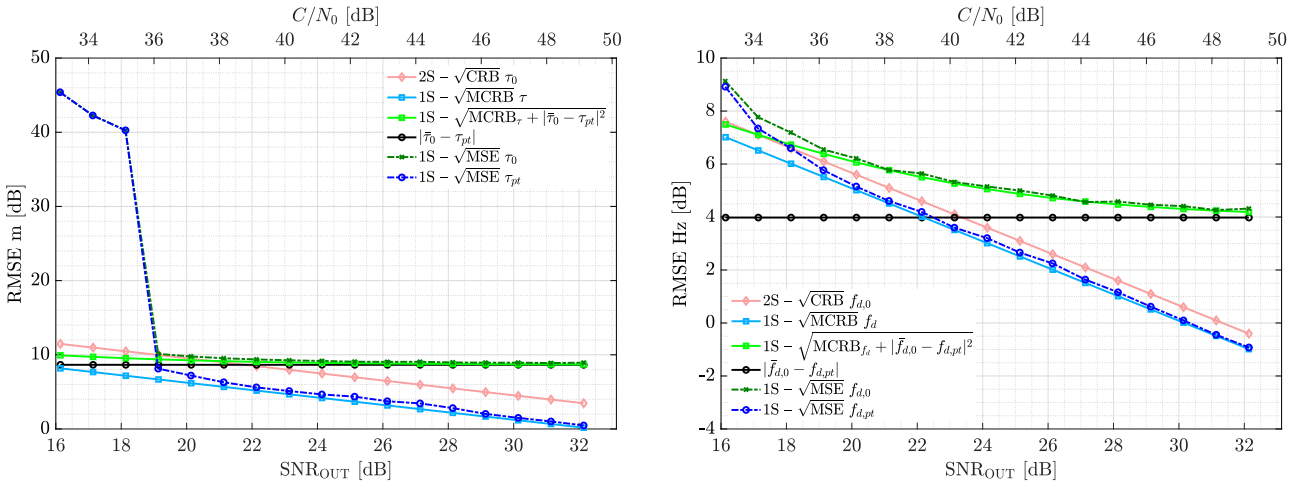

Figure 7: (b2) Misspecified CRB for delay (left) and Doppler effect (right) for $\Delta\bar{\tau} = 37$ m on GPS L1 C/A.

	Signal	Estimator	Bound	$\Delta\bar{\tau}$ (m)	$\bar{\rho}_1/\bar{\rho}_0$	$\Delta\bar{\phi}$ (°)	$\bar{f}_{d0}/\bar{f}_{d1}$ (Hz)
(b3)	Galileo E5	CRE	2S-CRB	37	0.5	180	10/6
(c1)	Galileo E5	CRE	2S-CRB	7	0.5	180	10/0.5
(c2)	Galileo E5	MMLE	MCRB	7	0.5	180	10/0.5

Table 5: Simulation scenarios for Galileo E5

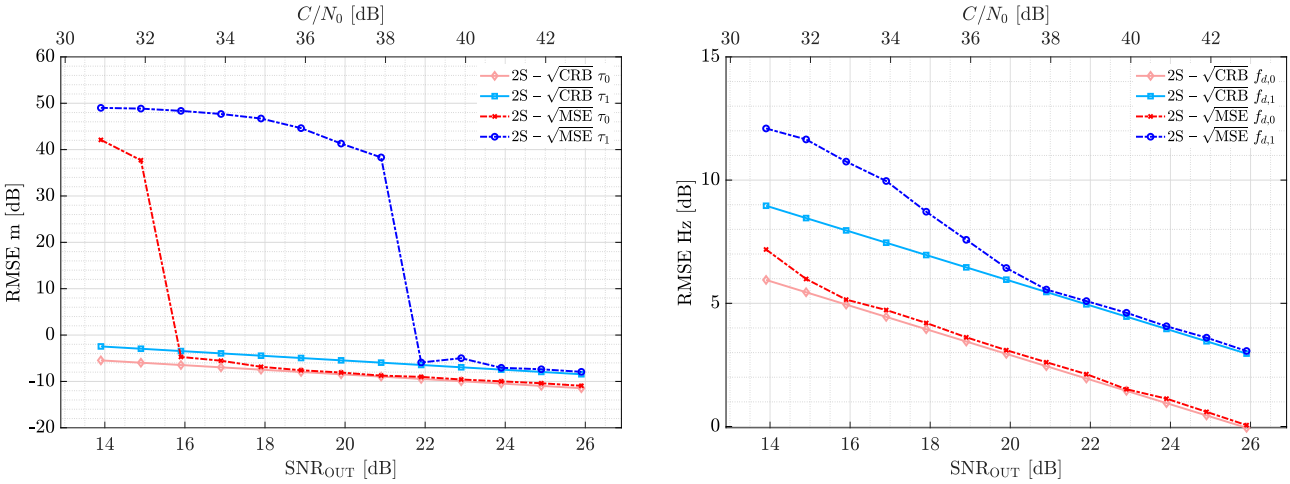

Figure 8: (b3) CRE mean square error for delay (left) and Doppler effect (right) with $\Delta\bar{\tau} = 37$ m on Galileo E5.

and multipath with scenario (c1) ($\Delta\bar{\tau} = 7$ m, $\Delta\bar{f}_d = -9.5$ Hz), the CRE again has difficulties in estimating the true parameters of the signal. Figure 9, shows that the CRE starts to be efficient only when both signals are well compensated. Even if the estimation performance and precision are better with Galileo E5 with respect to GPS L1 C/A, the convergence to the bounds on delay estimation arrives around 9 dB later than the convergence in scenario (b3). Nevertheless, the Doppler estimation is improved even when the multipath impacts the LOS signals with the highest ambiguity. It can be seen in Figure 9 that the CRE offers good performance in estimating the true Doppler of the LOS signal with a convergence to the CRB applied to $\bar{f}_{d0}$ even for the lower SNR regime.

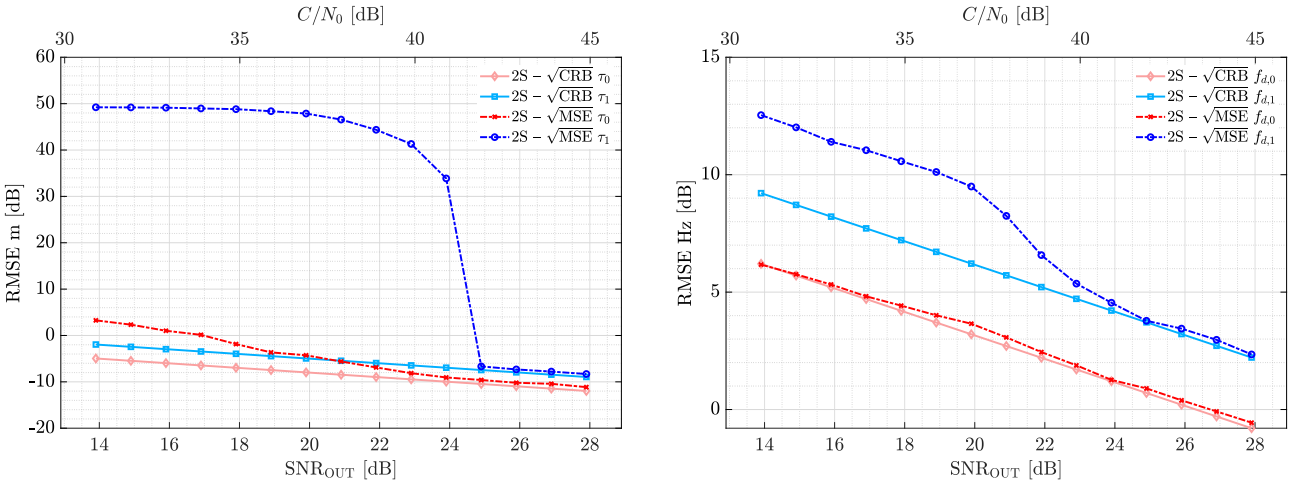

Figure 9: (c1) CRE mean square error for delay (left) and Doppler effect (right) with $\Delta\bar{\tau} = 7$ m on Galileo E5.

The study of the MCRB and the pseudotrue parameters is also very interesting to compare with GPS L1 C/A. With the latter, the delay estimation was limited to a precision of around 10 m and the Doppler estimate to a precision of around 2.25 Hz due to biased pseudotrue parameters. Now, using a Galileo E5, the delay estimation precision drops to 38 cm and the Doppler

estimation to a precision of 1.6 Hz in the high SNR regime. Moreover, a slower convergence appears on the evolution of the RMSE between $\mathrm{SNR}_{\mathrm{OUT}} = 15$ dB and 19 dB. This phenomenon can be explained by the presence of secondary peaks in the ACF as seen in Figure 3. For a specific noise power as well as a multipath scenario, secondary peaks can lead to an estimation error.

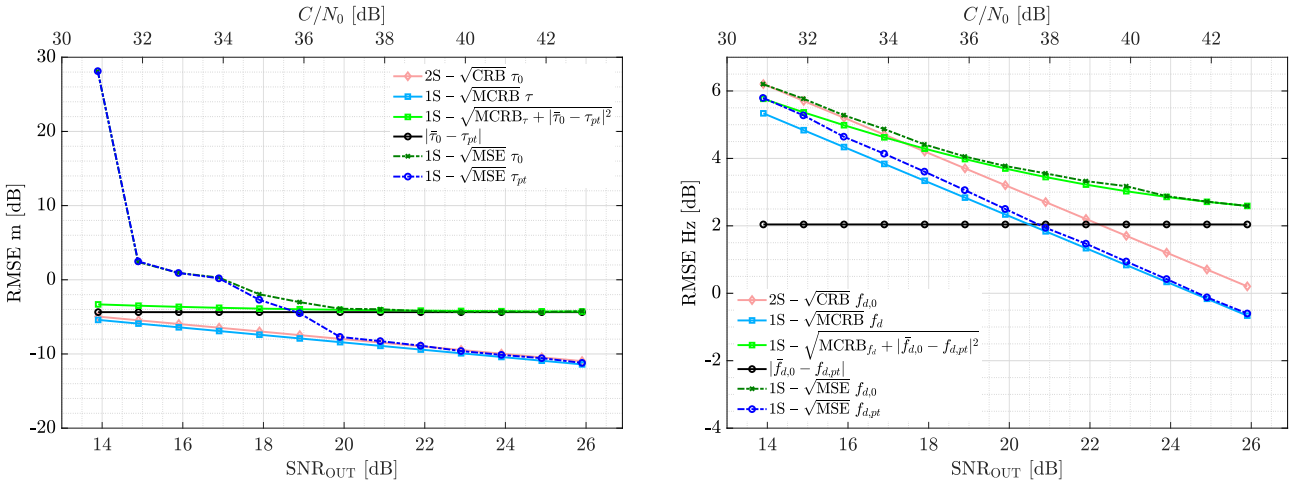

Figure 10: (c2) Misspecified CRB for delay (left) and Doppler effect (right) for $\Delta\bar{\tau} = 7$ m on Galileo E5.

4. Application to GPS L2-L5

	Signal	Estimator	Bound	$\Delta\bar{\tau}$ (m)	$\bar{\rho}_1/\bar{\rho}_0$	$\Delta\bar{\phi}$ (°)	$\bar{f}_{d0}/\bar{f}_{d1}$ (Hz)
(c3)	GPS L2-L5	MMLE	2S-CRB	7	0.5	180	10/0.5

Table 6: Simulation scenarios for GPS L2-L5

The previous scenario (c2), $\Delta\bar{\tau} = 7$ m and $\Delta\bar{f}_d = -9.5$ Hz, is now applied to GPS L2-L5 (c3). From a mitigation perspective, as the sampling frequency of GPS L2-L5 is higher than that of Galileo, it is easily assumed that CLEAN Relax will work with this signal. The convergence region may differ slightly. However, as explained earlier, it is too heavy to compute. So, a focus is put on the analysis of the MCRB. Figure 11 shows that GPS L2-L5 does not bring any improvement in estimation precision for delay and Doppler effect. In the situation of a misspecified model, the bias is more important when using GPS L2-L5. Nevertheless, the orders of magnitude for the error standard deviations remain close to those of Galileo E5. Regarding the convergence of the delay estimation to the bounds, Figure 11 shows a slower convergence after $\mathrm{SNR}_{\mathrm{OUT}} = 15$ dB compared to the delay estimate of Galileo E5 in Figure 10. This phenomenon is explained by the high presence of secondary peaks in the ACF of GPS L2-L5. In fact, Figure 3 shows that they are higher and more numerous. However, when considering the estimation of the Doppler effect, in this scenario (c3), the MMLE seems to converge much slower to the bounds. It can be assumed that a very high $\mathrm{SNR}_{\mathrm{OUT}}$ is required to observe the convergence region.

5. Overview of the results

From the previous simulations, some results of interest are recalled in Table 7. The successes of mitigating the multipath situation thanks to the CRE are indicated along with the limits of the performances of the MMLE to estimate the time-delay and Doppler frequency.

Scenario			GPS L1 C/A		Galileo E5		GPS L2-L5
			CRE	MMLE	CRE	MMLE	MMLE
(a)	$\Delta\bar{\tau} = 586$ m	$\Delta f_d = 10$ Hz	✓	-	-	-	-
(b)	$\Delta\bar{\tau} = 37$ m	$\Delta f_d = -4$ Hz	✗	6 m, 2.25 Hz	✓	-	-
(c)	$\Delta\bar{\tau} = 7$ m	$\Delta f_d = -9.5$ Hz	-	-	✗	37 cm, 1.6 Hz	43 cm, 2.6 Hz

Table 7: Overview of all simulation results: multipath mitigation success and performances limit of the MMLE.

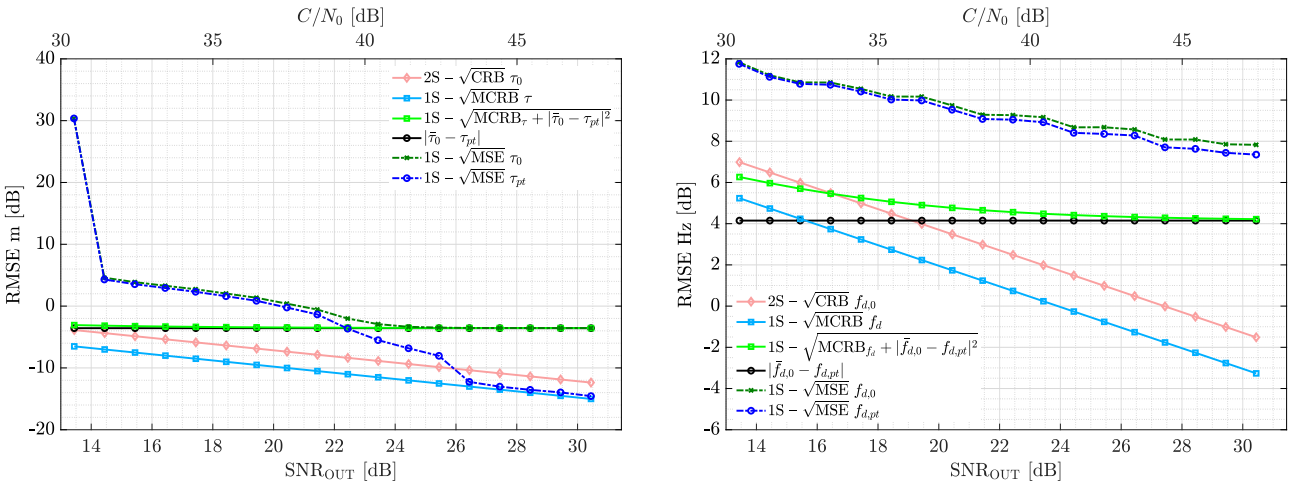

Figure 11: (c3) Misspecified CRB for delay (left) and Doppler effect (right) for $\Delta\bar{\tau} = 7$ m on GPS L2-L5.

VII. CONCLUSIONS

In this paper, the compact closed-form CRB for delay, Doppler, amplitude, and phase estimation derived in (Lubeigt et al., 2020) for a signal in the presence of a multipath was applied to the case of meta-signals. This compact closed form leads to an easy-to-use function of the CLRB depending on the baseband signal samples. Thus, a first apprehension of the robustness of the meta-signal against multipath can be appreciated through the computed CRB for time-delay and Doppler estimation. Indeed, for the special case of the delay estimation, it appeared that the CRBs of the meta-signals were significantly lower than the CRBs of the conventional signals. The misspecified CRB was also studied to assess the real estimation performances of a receiver using meta-signal in the presence of a single multipath. From this perspective, using meta-signal increases also significantly the estimation performances by reducing the bias induced by the pseudotrue parameters. So, meta-signals are more robust to multipath than conventional GNSS signals. However, between meta-signals, such as GPS L2-L5 and Galileo E5, it appeared that there was no major evolution by using one or the other. Moreover, in a situation with multipath, the scope of this paper shows a limit of delay estimation of dozens of centimeters.

In the practical situation of this contribution, this conclusion on GPS L2-L5 could be explained by the presence of high secondary peaks in the autocorrelation function of the signal, as well as the small difference in the sharpness of the main peak compared to the difference with GPS L1 C/A. Thus, to improve the comparison between meta-signals, wider signals such as GPS L1-L5 or Galileo E5-E1 could be considered. Meta-signals with more than two conventional signals could also be a promising way to increase robustness in harsh environment along with an improvement in the estimation precision. However, dealing with these signals may require very high computational resources as a result of the sampling frequency required to digitalize these signals.

Finally, future work is to be done to express the meta-signal thanks to a wideband model (Das et al., 2020). This model takes into account the impact of the Doppler effect on the code delay. Then, it may be interesting to suggest a compact-closed form of the Cramér-Rao Lower Bound for wideband signals. This modeling may help to identify the applicability domain of the narrowband assumption for meta-signals, notably for extra-wideband meta signals, or in high Doppler scenarios, such as low-Earth orbit satellite positioning.

APPENDIX

A. BOUNDS DERIVATION TERMS

for the sake of completeness, the definitions of the terms found in the close-form expression of the CRB are recaptured here.

$$\mathbf{s} = \left(\ \dots \quad s(nT_s) \quad \dots \ \right)^T_{N_1 \le n \le N_2}, \tag{43}$$

$$\boldsymbol{\nu}(f) = \left(\ \dots \quad e^{j2\pi f n} \quad \dots \ \right)^T_{N_1 \le n \le N_2}, \tag{44}$$

$$\mathbf{U}(\Delta b) = \operatorname{diag}\left(\ \dots \quad e^{-j\omega_c \Delta b n T_s} \quad \dots \ \right)_{N_1 \le n \le N_2}, \tag{45}$$

$$\mathbf{D} = \left(\ \dots \quad n \quad \dots \ \right)^T_{N_1 \le n \le N_2}, \tag{46}$$

$$\mathbf{V}^{\Delta,0}\left(\frac{\Delta\tau}{T_s}\right) = \int_{-\frac{1}{2}}^{\frac{1}{2}} \boldsymbol{\nu}(f)\boldsymbol{\nu}^H(f) e^{-j2\pi f \frac{\Delta\tau}{T_s}} \mathrm{d}f, \tag{47}$$

$$\left[\mathbf{V}^{\Delta,0}\left(\frac{\Delta\tau}{T_s}\right)\right]_{k,l} = \operatorname{sinc}\left(k - l - \frac{\Delta\tau}{T_s}\right),$$

$$\mathbf{V}^{\Delta,1}\left(\frac{\Delta\tau}{T_s}\right) = j2\pi \int_{-\frac{1}{2}}^{\frac{1}{2}} f\boldsymbol{\nu}(f)\boldsymbol{\nu}^H(f) e^{-j2\pi f \frac{\Delta\tau}{T_s}} \mathrm{d}f, \tag{48}$$

$$\left[\mathbf{V}^{\Delta,1}\left(\frac{\Delta\tau}{T_s}\right)\right]_{k,l} = \frac{1}{k - l - \frac{\Delta\tau}{T_s}} \left(\cos\left(\pi(k - l - \frac{\Delta\tau}{T_s})\right) - \operatorname{sinc}\left(k - l - \frac{\Delta\tau}{T_s}\right)\right),$$

$$\mathbf{V}^{\Delta,2}\left(\frac{\Delta\tau}{T_s}\right) = 4\pi^2 \int_{-\frac{1}{2}}^{\frac{1}{2}} f^2\boldsymbol{\nu}(f)\boldsymbol{\nu}^H(f) e^{-j2\pi f \frac{\Delta\tau}{T_s}} \mathrm{d}f, \tag{49}$$

$$\left[\mathbf{V}^{\Delta,2}\left(\frac{\Delta\tau}{T_s}\right)\right]_{k,l} = \pi^2 \operatorname{sinc}\left(k - l - \frac{\Delta\tau}{T_s}\right) + 2\frac{\cos\left(\pi(k - l - \frac{\Delta\tau}{T_s})\right) - \operatorname{sinc}\left(k - l - \frac{\Delta\tau}{T_s}\right)}{\left(k - l - \frac{\Delta\tau}{T_s}\right)^2}.$$

The proof of the previous equation can be found in (Lubeigt et al., 2020, Appendix A.2).

B. DIFFERENTIAL TERMS

The $\mathbf{Q}_q$ matrices are obtained from the second derivative of the continuous-time expression $a(t;\boldsymbol{\eta}) = s(t-\tau)e^{j\omega_c b(t-\tau)}$. In matrix form, this derivative is:

$$\frac{\partial^2 \alpha a(t;\boldsymbol{\eta})}{\partial\boldsymbol{\theta}\partial\boldsymbol{\theta}^T} = [\mathbf{Q}_1\mathbf{Q}_2\mathbf{Q}_3\mathbf{Q}_4]\left(\mathcal{D}^{(2)}(t;\boldsymbol{\eta}) \otimes \boldsymbol{I}_4 e^{-j\omega_c b(t-\tau)}\right) \tag{50}$$

with

$$\mathbf{Q}_1 = \begin{bmatrix} -\alpha\omega_c^2 b^2 & 0 & 0 & -j2\alpha\omega_c b & 0 & \alpha \\ j\alpha\omega_c & \alpha\omega_c^2 b & 0 & 0 & j\omega_c & 0 \\ je^{j\phi}\omega_c b & 0 & 0 & -e^{j\phi} & 0 & 0 \\ -\alpha\omega_c & 0 & 0 & -j\alpha & 0 & 0 \end{bmatrix} \quad \mathbf{Q}_2 = \begin{bmatrix} j\alpha\omega_c & \alpha\omega_c^2 b & 0 & 0 & j\alpha\omega_c & 0 \\ 0 & 0 & -\alpha\omega_c^2 & 0 & 0 & 0 \\ 0 & je^{j\phi}\omega_c & 0 & 0 & 0 & 0 \\ 0 & -\alpha\omega_c & 0 & 0 & 0 & 0 \end{bmatrix}$$

$$\mathbf{Q}_3 = \begin{bmatrix} je^{j\phi}\omega_c b & 0 & 0 & -e^{j\phi} & 0 & 0 \\ 0 & -je^{j\phi}\omega_c & 0 & 0 & 0 & 0 \\ 0 & 0 & 0 & 0 & 0 & 0 \\ je^{j\phi} & 0 & 0 & 0 & 0 & 0 \end{bmatrix} \quad \mathbf{Q}_4 = \begin{bmatrix} -\alpha\omega_c b & 0 & 0 & -j\alpha & 0 & 0 \\ 0 & \alpha\omega_c & 0 & 0 & 0 & 0 \\ je^{j\phi} & 0 & 0 & 0 & 0 & 0 \\ -\alpha & 0 & 0 & 0 & 0 & 0 \end{bmatrix} \tag{51}$$

$$\mathcal{D}^{(2)}(t;\tau) = \begin{bmatrix} s(t-\tau) \\ (t-\tau)s(t-\tau) \\ (t-\tau)^2 s(t-\tau) \\ s^{(1)}s(t-\tau) \\ (t-\tau)s^{(1)}(t-\tau) \\ s^{(2)}s(t-\tau) \end{bmatrix} \tag{52}$$

REFERENCES

Beckmann, P. and Spizzichino, A. (1987). *The Scattering of Electromagnetic Waves From Rough Surfaces*. Artech House.

Betz, J. W. (2001). Binary offset carrier modulations for radionavigation. *Navigation*, 48(4):227–246.

Borio, D. (2023). Bicomplex Representation and Processing of GNSS Signals. *NAVIGATION: Journal of the Institute of Navigation*, 70(4).

Borio, D. (2024). A General Multi-Dimensional GNSS Signal Processing Scheme Based on Multicomplex Numbers. pages 2904–2925, Baltimore, Maryland.

Borio, D. and Susi, M. (2024). GNSS Meta-Signal Tracking Using a Bicomplex Kalman Filter. *NAVIGATION: Journal of the Institute of Navigation*, 71(4):navi.674.

Camps, A., Park, H., Valencia i Domènech, E., Pascual, D., Martin, F., Rius, A., Ribo, S., Benito, J., Andrés-Beivide, A., Saameno, P., Staton, G., Martín-Neira, M., D'Addio, S., and Willemsen, P. (2014). Optimization and Performance Analysis of Interferometric GNSS-R Altimeters: Application to the PARIS IoD Mission. *IEEE Journal of Selected Topics in Applied Earth Observations and Remote Sensing*, 7(5):1436–1451.

Das, P., Ortega, L., Vilà-Valls, J., Vincent, F., Chaumette, E., and Davain, L. (2020). Performance limits of gnss code-based precise positioning: Gps, galileo & meta-signals. *Sensors*, 20(8):2196.

Das, P., Vilà-Valls, J., Vincent, F., Davain, L., and Chaumette, E. (2020). A New Compact Delay, Doppler Stretch and Phase Estimation CRB with a Band-Limited Signal for Generic Remote Sensing Applications. *Remote Sensing*, 12:2913.

Dovis, F. (2015). *GNSS interference threats and countermeasures*. Artech House.

Fortunati, S., Gini, F., and Greco, M. (2018). Chapter 4 - Parameter bounds under misspecified models for adaptive radar detection. In Chellappa, R. and Theodoridis, S., editors, *Academic Press Library in Signal Processing, Volume 7*, pages 197–252. Academic Press.

Fortunati, S., Gini, F., Greco, M. S., and Richmond, C. D. (2017). Performance bounds for parameter estimation under misspecified models: Fundamental findings and applications. *IEEE Signal Process. Mag.*, 34(6):142–157.

Fortunati, S. and Ortega, L. (2024). On the efficiency of misspecified Gaussian inference in nonlinear regression: application to time-delay and Doppler estimation. *Signal Processing*, 225:109614.

Germain, O. and Ruffini, G. (2006). A Revisit to the GNSS-R Code Range Precision.

Ghizzo, E. (2025). *Impact du leurrage sur le traitement du signal d'un récepteur GNSS*. PhD Thesis, Ecole Nationale de l'Aviation Civile.

Issler, J.-L., Paonni, M., and Eissfeller, B. (2010). Toward centimetric positioning thanks to L- and S-Band GNSS and to meta-GNSS signals. In *2010 5th ESA Workshop on Satellite Navigation Technologies and European Workshop on GNSS Signals and Signal Processing (NAVITEC)*, pages 1–8, Netherlands. IEEE.

Kaplan, E. D. and Hegarty, C. J. (2017). *Understanding GPS/GNSS: principles and applications*. Artech house, 3rd ed edition.

Kay, S. M. (1993). *Fundamentals of Statistical Signal Processing: Estimation Theory*. Prentice-Hall, Englewood Cliffs, New Jersey, USA.

Lestarquit, L., Artaud, G., and Issler, J.-L. (2008). AltBOC for Dummies or Everything You Always Wanted to Know About AltBOC. In *Proceedings of the 21st International Technical Meeting of the Satellite Division of The Institute of Navigation (ION GNSS 2008)*, pages 961–970.

Li, J. and Stoica, P. (1996). Efficient mixed-spectrum estimation with applications to target feature extraction. *IEEE Transactions on Signal Processing*, 44(2):281–295.

Lubeigt, C., L. Ortega, Vilà-Valls, J., and Chaumette, E. (2023). Untangling First and Second Order Statistics Contributions in Multipath Scenarios. *Signal Processing*, 205:108868.

Lubeigt, C., Ortega, L., Vilà-Valls, J., and Chaumette, E. (2023). Band-limited impulse response estimation performance. *Signal Processing*, 208:108998.

Lubeigt, C., Ortega, L., Vilà-Valls, J., Lestarquit, L., and Chaumette, E. (2020). Joint Delay-Doppler Estimation Performance in a Dual Source Context. *Remote Sensing*, 12(23):3894.

Lubeigt, C., Ortega Espluga, L., Vilà-Valls, J., Lestarquit, L., and Chaumette, E. (2022). Multipath Estimating Techniques Performance Analysis. Pages: 6.

Medina, D., Ortega, L., Vilà-Valls, J., Closas, P., Vincent, F., and Chaumette, E. (2020). A New Compact CRB for Delay, Doppler and Phase Estimation - Application to GNSS SPP & RTK Performance Characterization. *IET Radar, Sonar & Navigation*.

Morton, Y. J., Van Diggelen, F., Spilker Jr, J. J., Parkinson, B. W., Lo, S., and Gao, G. (2021). *Position, Navigation, and Timing Technologies in the 21st Century, Volumes 1 and 2*. John Wiley & Sons.

Ortega, L., Medina, D., Vilà-Valls, J., Vincent, F., and Chaumette, E. (2020). Positioning Performance Limits of GNSS Meta-Signals and HO-BOC Signals. *Sensors*, 20(12):3586.

Ortega, L., Poulliat, C., Boucheret, M., M.Aubault-Roudier, and Al-Bitar, H. (2018). New Solutions on the Design of a Galileo Acquisition-Aiding Signal to Improve the TTFF and the Sensitivity. In *ION International Technical Meeting of The Institute of Navigation (ITM 2018), USA, 29/01/18-01/02/18*. Institute of Navigation (ION).

Ortega Espluga, L. (2025). *Habilitation à Diriger des Recherches: Statistical Signal Processing for the Design of Navigation and Localization Systems*. PhD thesis, Université Toulouse 3 Paul Sabatier.

Ottersten, B., Viberg, M., Stoica, P., and Nehorai, A. (1993). Exact and large sample maximum likelihood techniques for parameter estimation and detection in array processing. In Haykin, S., Litva, J., and Shepherd, T. J., editors, *Radar Array Processing*, chapter 4, pages 99–151. Springer-Verlag, Heidelberg.

Paonni, M. and Bavaro, M. (2013). On the Design of a GNSS Acquisition Aiding Signal. Proc. of the ION GNSS+,.

Paonni, M., Curran, J. T., Bavaro, M., and Fortuny-Guasch, J. (2014). GNSS Meta-signals: Coherently Composite Processing of Multiple GNSS Signals.

Rebeyrol, E. (2007). *Galileo signals and payload optimization*. PhD thesis, Telecom ParisTech Paris, France.

Renaux, A., Forster, P., Chaumette, E., and Larzabal, P. (2006). On the High-SNR Conditional Maximum-Likelihood Estimator Full Statistical Characterization. *IEEE Trans. Signal Process.*, 54(12):4840 – 4843.

Ribot, M. A., Botteron, C., and Farine, P. (2016). Derivation of the Cramér-Rao Bound in the GNSS-Reflectometry Context for Static, Ground-Based Receivers in Scenarios with Coherent Reflection. *Sensors*, 16(12):2063.

Rodríguez, J. (2008). *On Generalized Signal Waveforms for Satellite Navigation*. Universitätsbibliothek der Universität der Bundeswehr München.

Stoica, P. and Nehorai, A. (1990). Performance Study of Conditional and Unconditional Direction of Arrival Estimation. *IEEE Trans. Acoust., Speech, Signal Process.*, 38(10):1783–1795.

Teunissen, P. J. and Montenbruck, O. (2017). *Springer Handbook of Global Navigation Satellite Systems*. Springer Cham, Switzerland.

Teunissen, P. J. G. and Montenbruck, O., editors (2017). *Handbook of Global Navigation Satellite Systems*. Springer, Switzerland.

Townsend, B. R., Fenton, P. C., Van Dierendonck, K. J., and Richard Van Nee, D. J. (1995). Performance Evaluation of the Multipath Estimating Delay Lock Loop. *Navigation*, 42(3):502–514.

Van Trees, H. L. (2001). *Part 1: Detection Estimation and Linear Modulation Theory*. Detection, Estimation, and Modulation Theory. Wiley.

Zhao, T. and Huang, T. (2016). Cramer-Rao Lower Bounds for the Joint Delay-Doppler Estimation of an Extended Target. *IEEE Transactions on Signal Processing*, 64(6):1562–1573.